ADVANCED MATERIALS
www.advmat.de

Natural Flexible Dermal Armor

Wen Yang, Irene H. Chen, Bernd Gludovatz, Elizabeth A. Zimmermann, Robert O. Ritchie, and Marc A. Meyers**

Fish, reptiles, and mammals can possess flexible dermal armor for protection. Here we seek to find the means by which Nature derives its protection by examining the scales from several fish (*Atractosteus spatula*, *Arapaima gigas*, *Polypterus senegalus, Morone saxatilis, Cyprinius carpio)*, and osteoderms from armadillos, alligators, and leatherback turtles. Dermal armor has clearly been developed by convergent evolution in these different species. In general, it has a hierarchical structure with collagen fibers joining more rigid units (scales or osteoderms), thereby increasing flexibility without significantly sacrificing strength, in contrast to rigid monolithic mineral composites. These dermal structures are also multifunctional, with hydrodynamic drag (in fish), coloration for camouflage or intraspecies recognition, temperature and fluid regulation being other important functions. The understanding of such flexible dermal armor is important as it may provide a basis for new synthetic, yet bioinspired, armor materials.

1. Introduction

Protective armor can be traced to Placoderm fossils found as many as 380 million years ago. Many dinosaurs possessed defensive armor, prime examples being the Stegosaurus. The clade of Thyreophora includes the Ankylosauria, huge herbivores that existed in the Late Cretaceous (99.6–65.5 Ma) as well as the Stegosauria. Prior to that, fish with bony scales, Ostracoderms, evolved in the Ordovican (~500 Ma).

Many current-day animals also possess armor. These include mammals (e.g., armadillos and pangolin), reptiles (e.g., alligators, crocodiles, lizards, turtles) and numerous fish. Four representative species (of both extinct and current-day species) are shown in **Figure 1**:[1–3] a dinosaur (*Edmontonia*), a mammal (*Dasypus novencinctus*, armadillo), a reptile (*Dermochelys coriacea*, leatherback turtle), and a fish (*Arapaima gigas*, arapaima). Despite the wide variation in the structure and composition of their armor, there is distinct commonality: the armor is composed of rigid plates connected to the body and to themselves by collagen fibers/muscles. In the case of the dinosaurs, these plates could be as thick as 100 mm. In other cases, such as the bichir that will be discussed in Section 3, the thickness is a few millimeters. In small fish, the scales can be fractions of a millimeter. The ratio of plate size to animal size can govern how flexible the armor is; generally, the lower the ratio, the greater the flexibility. In some cases, such as in adult sauropod dinosaurs from Madagascar, the osteoderms found isolated under the dermis served as an internal source of calcium.[4]

Fish have, for the most part, a dermal protection arrangement where the overlap of scales is prominent; this is somewhat different to osteoderms. This is a necessity of the fluid mechanics requirements to minimize drag in water. The surface topography of the dermal protection layer in terrestrial animals is not governed by the same limitations because of the much lower dynamic viscosity of air. Turtles,[5–7] armadillos,[8,9] alligators,[10,11] lizards[12–14] and other terrestrial animals tend to have juxtaposed plates that have different degrees of flexibility and are connected by collagen fibers. An exception is the pangolin,[15,16] which has overlapping keratin scales.

The scales of fish are classified into four groups: placoid,[17,18] ganoid,[18,19] cosmoid,[17,20–22] and elasmoid (cycloid and ctenoid).[23–25] These are shown in **Figure 2** together with illustrations indicating their arrangement and overlap. Placoid (Figures 2a[26],b) are typical scales of sharks or rays. They have a surface structure that generates small-scale vorticity in water, thereby decreasing drag.[27] The ganoid scales (Figures 2c,d) are composed of a thin surface layer of ganoine, akin in hardness to tooth enamel, riding on a softer but tougher bony foundation. These are the hardest scales in fish, and are characteristic of the Alligator gar (Figures 2c,d) and Senegal bichir. The elasmoid class consists of two kinds of scales, cycloid and ctenoid. They have similar shapes, but there are significant differences. For example, the outer surface of the cycloid is smooth while the ctenoid has a comb-like outer

W. Yang, I. H. Chen, Prof. M. A. Meyers
Materials Science and Engineering Program
University of California
San Diego, La Jolla, CA 92093, USA
E-mail: mameyers@eng.ucsd.edu
B. Gludovatz, E. A. Zimmermann, Prof. R. O. Ritchie
Department of Materials Science and Engineering
University of California
Berkeley, CA 94720
E-mail: roritchie@lbl.gov
Prof. R. O. Ritchie
Materials Sciences Division
Lawrence Berkeley National Laboratory
Berkeley, CA 94720
Prof. M. A. Meyers
Department of Mechanical and Aerospace Engineering and Nanoengineering
University of California
San Diego, La Jolla, CA 92093, USA

DOI: 10.1002/adma.201202713

surface. Some fish can have both cycloid and ctenoid scales as armor.

Table 1[9,10,19,28–36] shows representative animals and their different types and sizes of scales and osteoderms as well as their primary functions. The primary function of scales and osteoderm is to provide protection. However, these dermal structures are also multifunctional, with hydrodynamic drag (in fish),[37–38] coloration for camouflage or intraspecies recognition,[39] luminescence,[27,40] temperature[10,41] and fluid regulation[37] being other important functions. For example, the U-shaped valleys in a shark scale (Figure 2a) can reduce frictional drag by up to 8%[27,38] and are inspiring synthetic designs. Seidel[10] proposed that the bony plates of the stegosaurus could have served as heat absorbers like alligator osteoderms. In the *Rapetosaurus*, a dinosaur, calcium storage was an important additional function.[33]

2. Hierarchical Structure of Selected Animals

One of the main reasons that these small and lightweight scales are strong is their hierarchical structure. **Figure 3** shows schematic illustrations of the hierarchical structures of the dermal armors from three selected animals. *Arapaima gigas*, shown in Figure 3a, is one of the largest freshwater fish in the world and is native to the Amazon basin in South America.[42–44] In adults, the scales have dimensions of 50–100 mm in length and ~40 mm in width, and are composed of two layers: an external layer about 600 μm thick and an internal layer ~1000 μm thick. The external layer is highly mineralized with ridges, while the internal layer contains collagen fibers in orientations making an angle with each other that is in the range 60–75°. This configuration can produce the Bouligand[45] arrangement with the orientations describing a helicoid. This stacking of lamellae of parallel fibers is characteristic of ctenoid scale of teleost fish.[46–50] The diameter of the collagen fibers is around 1 μm, and they are comprised of collagen fibrils of roughly 100 nm in diameter. The arapaima scales overlap by more than 60% on the surface, which is far more than in the alligator gar where the scales only overlap by ~30% (Figure 3b).

The alligator gar scale (Figure 3b), a ganoid scale, also contains two layers. The outer layer, termed "ganoine", is ~600 μm thick (in adult specimens) and hard, being comprised of hydroxyapatite crystals; the inner layer is thicker (~3500 μm) and consists of a bone basal layer (these dimensions naturally scale with the size of the fish). Similar to the arapaima scale, the external ganoine layer is highly mineralized, providing a hard-protection barrier to external attack, whereas the inner bone layer with its collagen fibers provides a "soft/buffer" layer to promote toughness. However, as discussed below in Section 3, the mechanical properties are quite different from those of the cycloid and ctenoid scales.

Figure 3c shows the hierarchical structure of osteoderm[9] in the nine-banded armadillo (*Dasypus novemcinctus*). As the name suggests, osteoderms are the 'bony skin', found in the reptile orders Crocodilia (crocodiles, alligators, caimans) and Testudines (turtles, tortoises, terrapins), and in the mammal order Cingulata (armadillos). The length of the Texas armadillo (including the tail) is about 0.75 m and its carapace covers the head, pectoral, banded, pelvic shields and tail, leaving the soft belly unprotected. The epidermis is α-keratin and serves as a waterproofing layer. Below the epidermis, the osteoderms show three characteristic regions: an external dense bone, a central porous bone and an internal dense bone layer, as shown in the cross-sectional image in Figure 3c. This sandwich structure

Wen Yang is a postdoctoral researcher in the Materials Science and Engineering Program at the University of California, San Diego. She received the B.S. degree in Physics from Shenyang University of Technology, and M.S. and Ph.D. degrees in Materials Science from Northeastern University in China. Her research focuses on bioinspired materials and specifically on the relationship between structural characterization and mechanical behavior of biological materials.

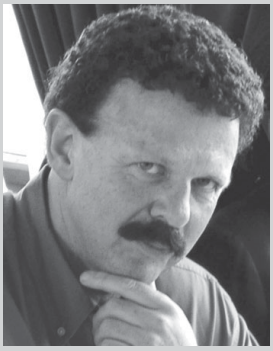

Robert O. Ritchie is the H.T. & Jessie Chua Distinguished Professor of Engineering in the Departments of Materials Science & Engineering and Mechanical Engineering at the University of California Berkeley; he is also Senior Faculty Scientist at the Lawrence Berkeley National Laboratory. He received B.A., M.A., Ph.D. and Sc.D. degrees in physics/materials science from Cambridge University, and is known for his research into the mechanics and mechanisms of fracture and fatigue of structural and biological materials. He is a member of the National Academy of Engineering, the U.K. Royal Academy of Engineering, and the Russian Academy of Sciences.

Marc André Meyers, Distinguished Professor in the Departments of Nanoengineering, and Mechanical and Aerospace Engineering, University of California San Diego, focuses his research in the mechanical behavior of materials.He is a graduate of the Federal Univeristy of Minas Gerais, a member of the Brazilian Academy of Sciences, and writes fiction.

Adv. Mater. **2012**,
DOI: 10.1002/adma.201202713

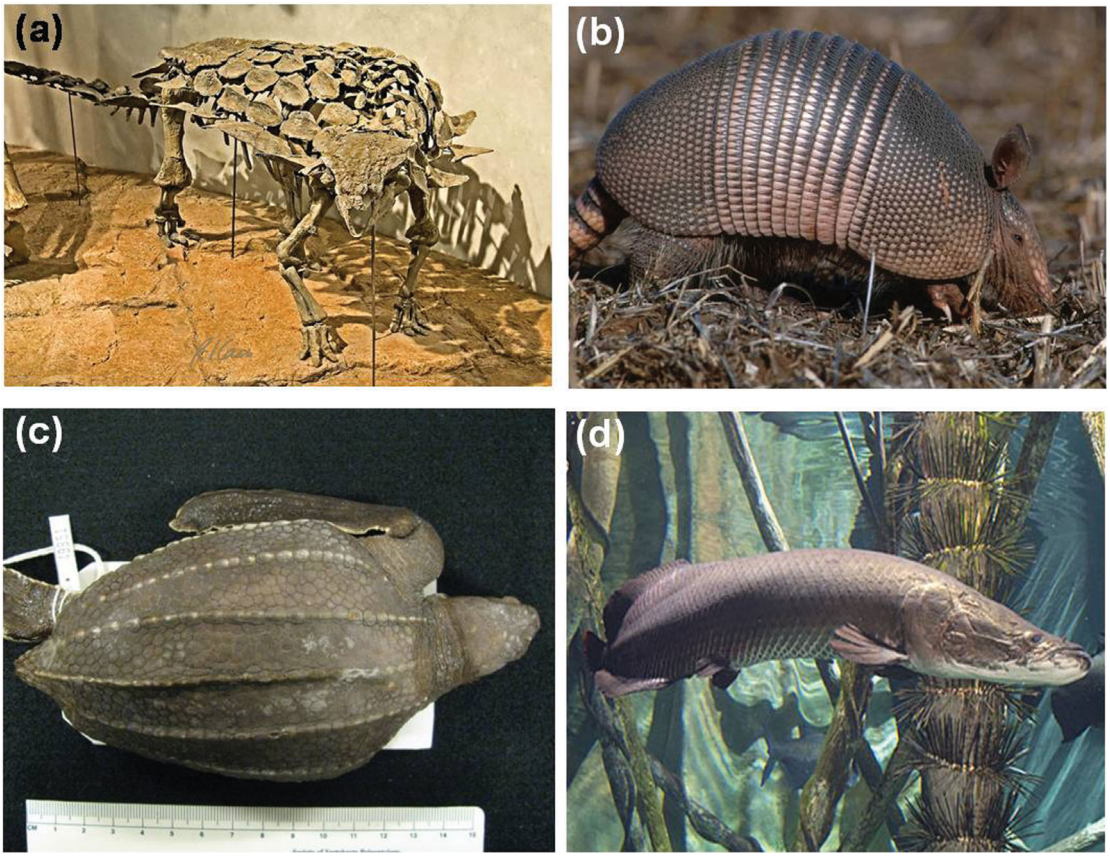

Figure 1. Animals with natural flexible dermal armor; (a) dinosaur skeleton (*Edmontonia*),[1] (b) armadillo (mammalia),[2] (c) leatherback turtle (reptile), (d) arapaima (fish).[3] Panel (a): Reproduced with permission.[1] Copyright 2012, Robert I Carr. Panel (b): Image courtesy of John and Karen Hollingsworth/USFWS. Panel (d): Reproduced with permission.[3] Copyright, Tennessee Aquarium.

(dense outer sheaths enclosing a porous core) is a configuration found in the structures of many animals requiring low density along with some energy absorption capability and stiffness (e.g., skulls, ribs). The osteoderms are hexagonally-shaped in the pectoral and pelvic regions and triangular-shaped in the banded shield (torso) region. In comparison to the mineralized collagen fibers in the tile,[9] non-mineralized collagen fibers (Sharpey's fibers) connect and hold the tiles together,[8] thereby providing flexibility. This structure provides a unique mechanism to protect the armadillo. In a live armadillo, these tiles are irrigated by blood and stronger than in the dry condition; the mineralized collagen fibers inside the osteoderms act to impede crack propagation through them, with the Sharpey's fibers ensuring the integrity and toughness of the tiling system.

3. Mechanical Design Principles of Natural Armor

3.1. Relationship Between Hierarchical Structure and Mechanical Properties

3.1.1. Fish Scales

The hierarchical structure and the unique junction of fish scales, discussed in Section 2, can provide an outstanding mechanical response. **Figures 4**,**5**[36] show the alligator gar scale in detail. The rhombic-shape scales (Figure 4a) arrange in rows with the junctions shown in brown (Figure 2c). Each scale has a ganoine external layer and a bony internal layer (Figure 4b). Figures 4c,d show the ganoine layer with rod-like hydroxyapatite (HAP) crystals of diameter ~60 nm arranged in different orientations marked as A-B-C-D. The bony internal layer contains HAP and mineralized collagen fibers with the characteristic of 67 nm periodicity (Figures 4e,f). Nanoindentation testing revealed that the hardness of ganoine and bone are 3.6 ± 0.3 GPa and 0.7 ± 0.1 GPa,[28] respectively, i.e., the ganoine is five times harder than bone. The compression strength of the bony component of scales (in the wet condition) is about 315 MPa and the corresponding Young's modulus is ~4 GPa. The collagen fibers provide flexibility and toughness to the bony part of the scales. In tension loading, the fibers separate from the mineral and often buckle; the links between them become stretched and eventually break.

There are characteristic features in the structure of the scale, one being the pattern of tubules, ~200 μm in diameter, in the center of the scale (Figure 5b), the other being the tubules and collagen fibers with 2–5 μm diameter embedded in the mineralized matrix (Figure 5e). The tubules and collagen fibers (from top-view) are more evident in the interior part of the bony layer (close to the fish skin, Figure 5d) than in the surface side (close to the ganoine, Figure 5c). The principal component of this natural armor is HAP which is naturally brittle and hence

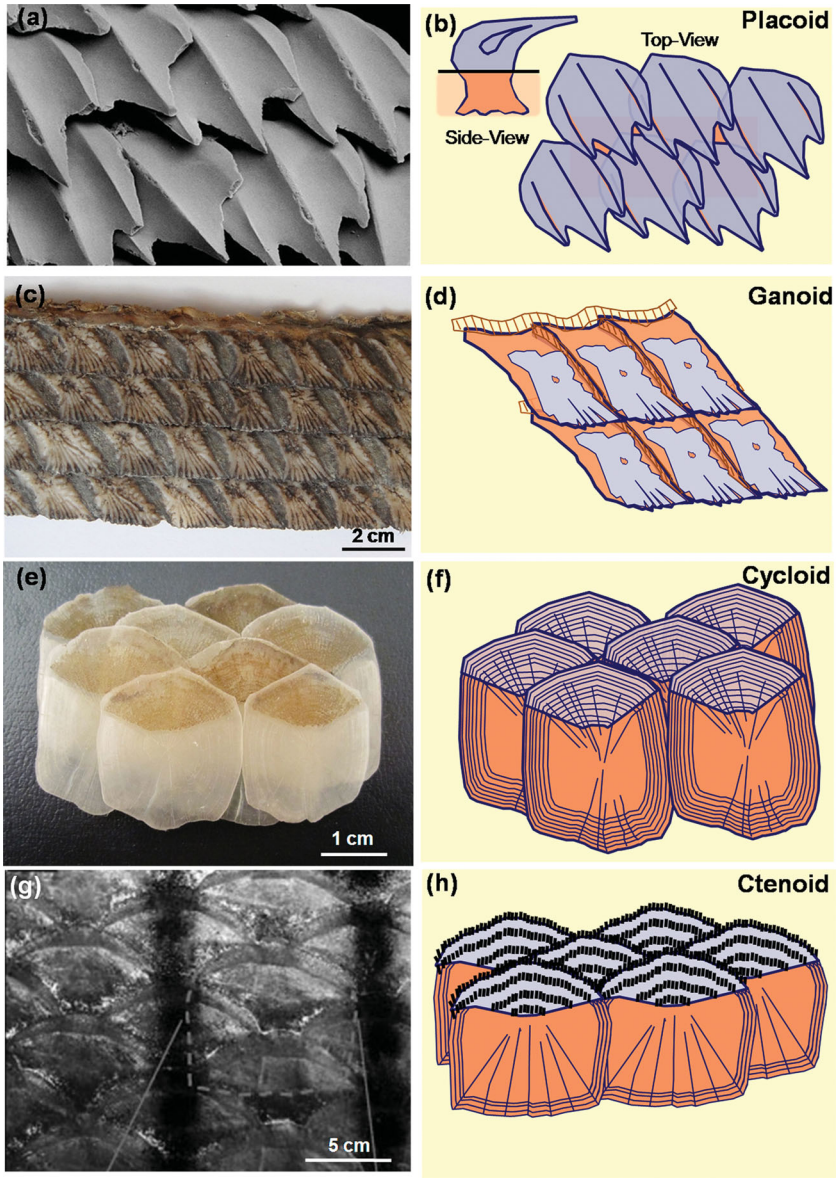

Figure 2. Different types of fish scales and their overlaps; (a)[26] and (b) placoid, (c) and (d) ganoid, (e) and (f) cycloid, (g)[25] and (h) ctenoid. (Cosmoid scales not shown). Panel (a): Reproduced with permission.[26] (Image of placoid scale: Sue Lindsey, copyright, The Australian Museum.) Panels g): Reproduced with permission.[25]

Table 1. Animals and their natural dermal armor. Adapted from Ref. [34] with permission. Copyright 2002, Springer.

Animal	Size of Animal		Size of Scales (mm)	Layers	Young's modulus [GPa]	Functionality
	Length (m)	Weight (kg)				
Alligator	4	~360	31–43	Bone	0.5[35]	Protection, regulation of body temperature[10]
Gar	2.4–3	~100	10–40	Ganoine Bone	3.5–5.2*[36]	Protection (ganoine); buffered and flexible to the skin (bone)
Arapaima	2–2.5	~100	40–100	Mineralized collagen	1.2 ± 0.2[28]	Protection (external); flexibility and toughness (internal)[28]
Bichir	0.05–0.12 (young)	0.1–0.3[30]	2.5–5	Ganoine Dentin	17[19]	Protection from biting attack[31,32]
	0.23–0.24 (adult)[29]			Isopedine Bone		
Armadillo	0.5–1	5.4–10	~5	Bone	0.43[9]	Protection[9]
Leatherback turtle	1.8–2.2	250–700	30–50	Bone	—	
Dinosaur Rapetosaurus	15		300	Bone		Protection, calcium storage[33]

*Young's modulus of gar scale was obtained from compression in different orientations and analyzed by Weibull methods.

Adv. Mater. **2012**,
DOI: 10.1002/adma.201202713

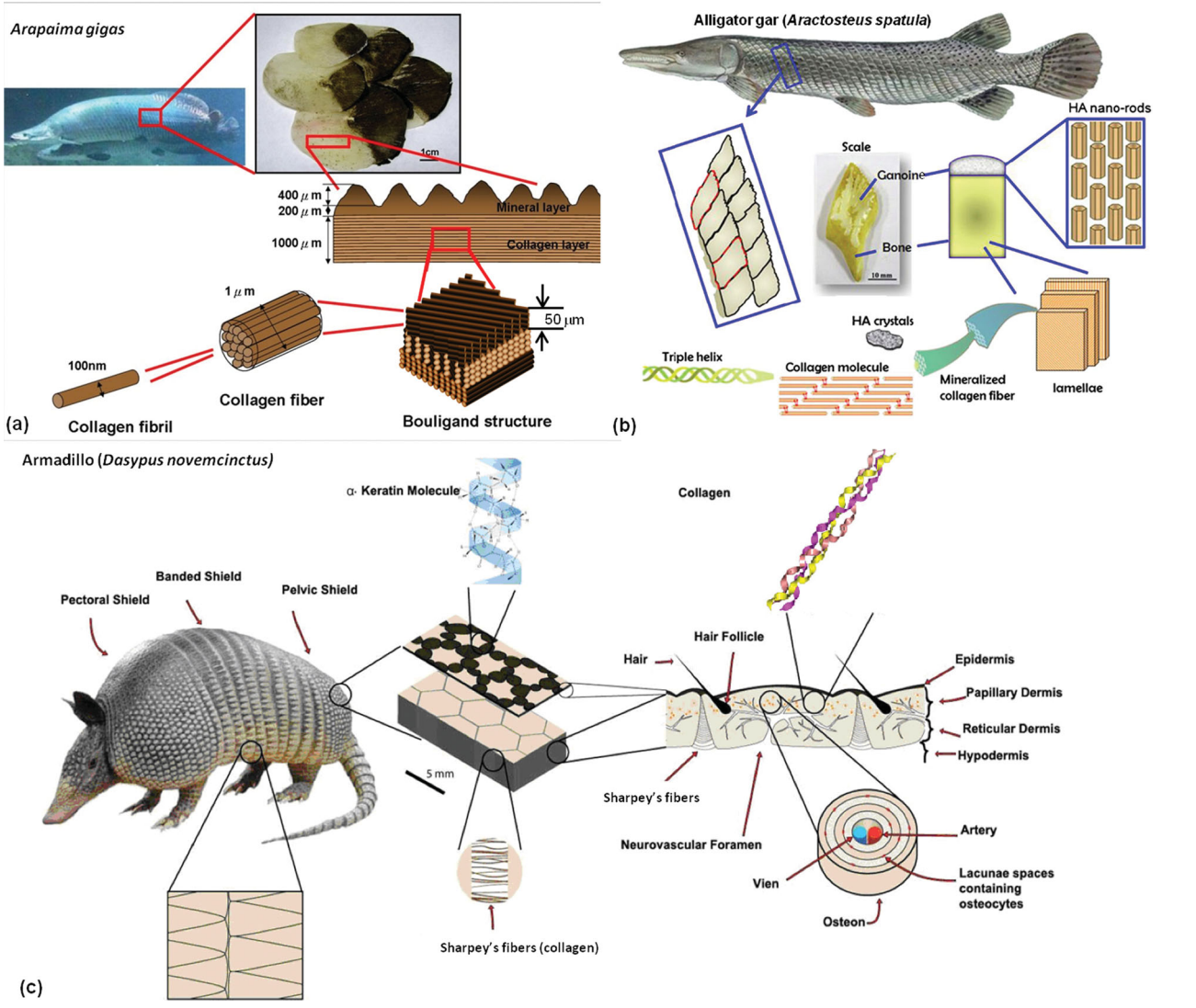

Figure 3. Hierarchical structure of dermal armor for three animals; (a) *Arapaima gigas* (Adapted with permission from Ref. [28]. Copyright 2012, Cambridge University Press), (b) *Atractosteus spatula* (reproduced with permission from Ref. [28]. Copyright 2012, Cambridge University Press), (c) *Dasypus novemcinctus* (reproduced with permission from Ref. [28]. Copyright 2011, Elsevier).

prone to crack; however, when HAP is combined with collagen fibers (cross-sectional view shown in Figure 5f), a hierarchical structure is formed that is enhanced by junctions that create a redistribution of loads on the surface, decreasing the stress concentration from a bite.

Figure 6 shows more details of the arapaima scales. Figures 6a,b show the overlapped scales with the exposed (E) and covered, or overlapped (C), portions. These five overlapped scales represent a portion of the dermal protection, seen more clearly in Figure 6b. At a higher magnification, the mineralized ridges of the scales become visible (Figures 6c-f); they are thicker and less regular in the exposed parts of the scales, E. The less mineralized portion of the scale is comprised of superposed lamellae (Figure 3a). There are at least three orientations of collagen fibers; they become separated during tensile testing such that bundles of them can be seen in the images (Figures 6g,h). Fiber terminations remaining on the fracture surface are curled up (Figure 6h), indicative of tensile extension prior to fracture. This cross-ply arrangement of fibers is effective in providing in-plane isotropy of strength to the scales. **Figure 7** shows a polished section of the scale at (a) low and (b) higher magnifications; the lamellae are visible with the external layer consisting of highly mineralized ridges. The internal layers (Figure 7b) have a crack pattern that is produced by shrinkage during drying. This crack pattern can be used to obtain an approximate idea of the misorientation between the layers. If the fibers are parallel to the section plane, no cracking will be observed; however, if every second layer is uncracked, the misorientation angle is ~90°, whereas if every third layer is uncracked, this angle is ~60°.

The ganoid scale of *Polypterus senegalus* (Senegal bichir) has four layers, shown in **Figure 8**:[19] ganoine, an enamel-like

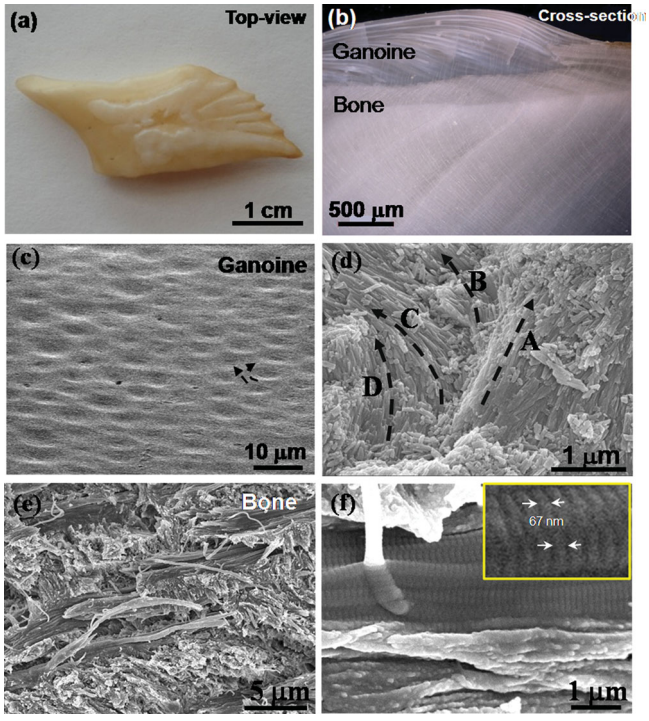

Figure 4. Structural characterization of alligator gar (*Atractosteus spatula*) scale;[36] (a) top-view of scale, (b) cross-section of scale showing ganoine (outer layer) and bone (inner layer), (c) cross-section of ganoine, (d) mineral crystals in ganoine (note different orientations), (e) mineral and collagen fibers in bone, (e) parallel collagen fibers showing characteristic 67 nm banding.

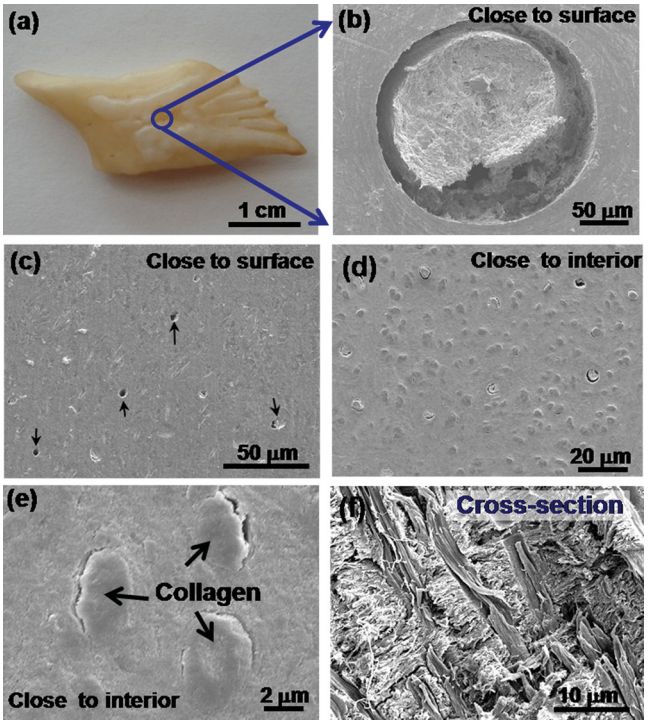

Figure 5. Tubules and collagen fibers in alligator gar (*Atractosteus spatula*) scale;[36] (a) top-view of scale, (b) a big tubule in the center of the scale, (c) tubules (marked by arrows) in bone layer close to the ganoine (top-view), (d) tubules and collagen fibers in the bone layer (top-view), (e) polished surface showing 2–5 μm collagen fibers (top-view), (f) collagen fibers observed from the cross-section.

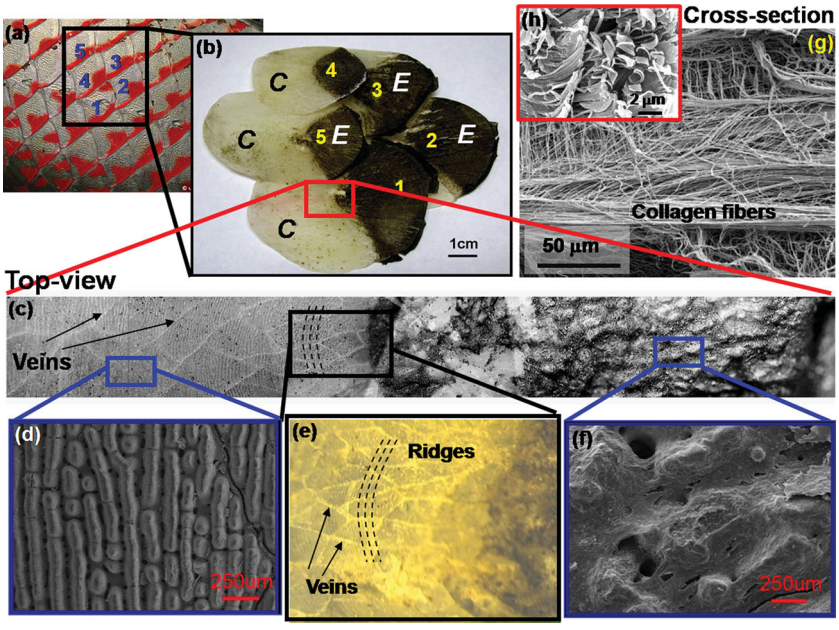

Figure 6. Structural characterization of arapaima (*Arapaima gigas*) scale; (a) overlapped scales, (b) enlarged view of scales showing covered (C) and exposed (E) parts, (c) top-view of the scale from the covered part to the exposed part, (d) surface of covered part, (e) the region between the covered and exposed surface in the center of the scale containing veins and ridges, (f) exposed portion of the scale, (g) collagen fibers in separated configuration, (h) SEM image of fractured fibers in tensile specimen. Adapted with permission.[44]

Adv. Mater. **2012**,
DOI: 10.1002/adma.201202713

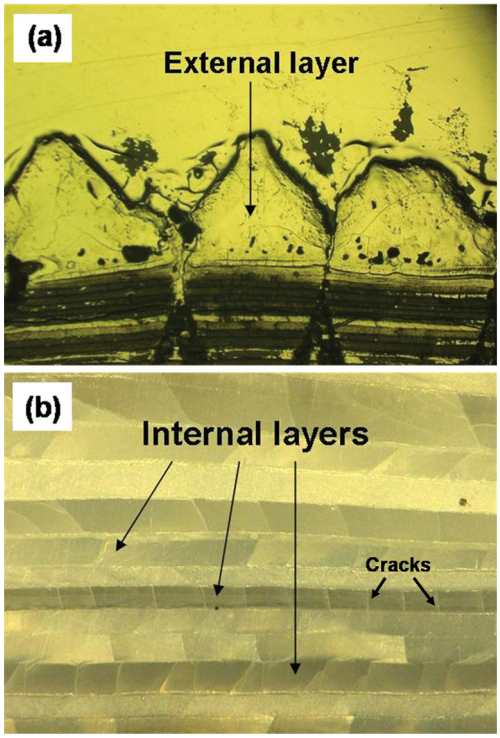

Figure 7. Cross-section of arapaima scale (from Figure 4b and 4c in Ref. [43], reproduced with permission, Copyright 2011, Elsevier); (a) low magnification showing external layer that is highly mineralized with an internal lamellar arrangement of collagen fibers, (b) higher magnification view of internal layer with cracks produced by drying.

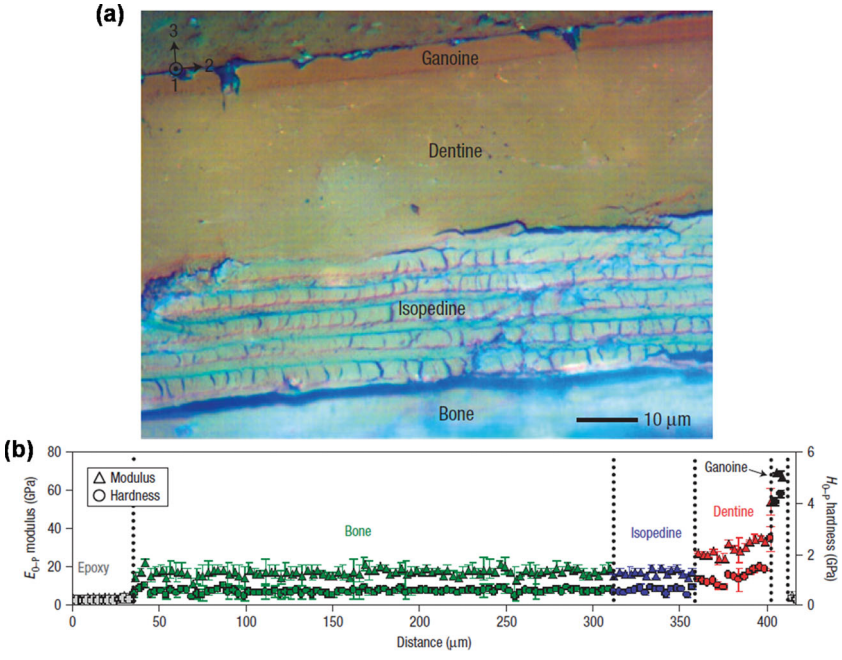

Figure 8. Cross-sectional view of Senegal bichir scale and hardness of layers (from Figures 1d and 2a in Ref. [19], reproduced with permission, Copyright 2008, Nature Publishing Group); (a) cross-section showing four different layers (ganoine, dentine, isopedine and bone); note that isopedine is formed by lamellae, (b) nanoindentation hardness and Young's modulus as a function of distance from inner layer (bone) to outer layer (ganoine) across the cross-section.

hydroxyapatite, dentine, isopedine-which appears to form layers in an analogous manner to the lamellae of teleosts, and bone – the foundation and major constituent. The hardness, as measured by nanoindentation, decreases from the surface to the interior, a common feature of all scales. The ganoine layer is composed of rod-like HAP nanocrystals arranged perpendicular to the surface; they are thinner than those in alligator gar scale with a length of ~220 nm and diameter of ~40 nm.

To examine the mechanical response of the ganoine layer, microscale pillar experiments were performed by Han et al.[51] by applying the flat punch of a nanoindenter to a cylindrical specimen with the surroundings etched away. Specimens, of diameter ~2 μm with a height of a few micrometers, were prepared along three orientations (0°, 45°, and 90° to surface), with the HAP crystals normal to the surface. Loading with the force direction aligned with the crystals gave the highest strength, while loading at 45° gave the lowest, with the fracture path showing a preference for intercrystal separation, as shown in the schematic drawings in **Figure 9**.[51] These experiments demonstrate the utility of the materials science testing methodology in revealing important attributes of these layers. The structure and orientation of the rods are such that they promote a shear cracking path to cause fracture.

Carp and striped bass have scales that are cycloid. The cross-section of a carp scale is shown in **Figures 10**a–c.[52] The external layer is highly mineralized with no collagen lamellae. Below this layer, however, a classic lamellar structure can be seen, with layer thickness of ~30 μm where, under transmission electron microscopy (TEM), individual fibrils and interfibrillar minerals can be detected. The characteristic pattern of the collagen, with 67 nm periodicity associated with the spacing of the mineral, can be seen in Figure 10b; Figure 10c shows their cross-section with fibrils of ~100 nm in diameter as well as interfibrillar minerals that appear darker. In comparison, a corresponding transmission electron microscopy (TEM) micrograph of several layers in the scale of *Pagrus major* (sea bream) shows the cross-ply nature of sequential collagen layers (Figure 10d).[46]

The uniaxial tensile strengths of scales of different fish are compared in **Figure 11**;[25,36,43,52] four or five tests, all in the wet condition, are shown in each plot to illustrate the variability. The ultimate strength of the alligator gar scales (~100 MPa) is around three times that of the other three scales (~30 MPa). This is the direct result of the bony structure in the ganoid scale of the alligator gar in contrast with the lamellar collagen structure of the other scales. Ikoma et al.[46] reported an ultimate strength of 93 MPa for *Pagrus major* (a teleost fish); however, these tests were performed dry and there is a very significant effect of hydration on the strength of the scales. Zhu et al.[25] performed uniaxial tensile tests which showed some effect of orientation with angles of 45° and 90° from the longitudinal axis of the fish having higher

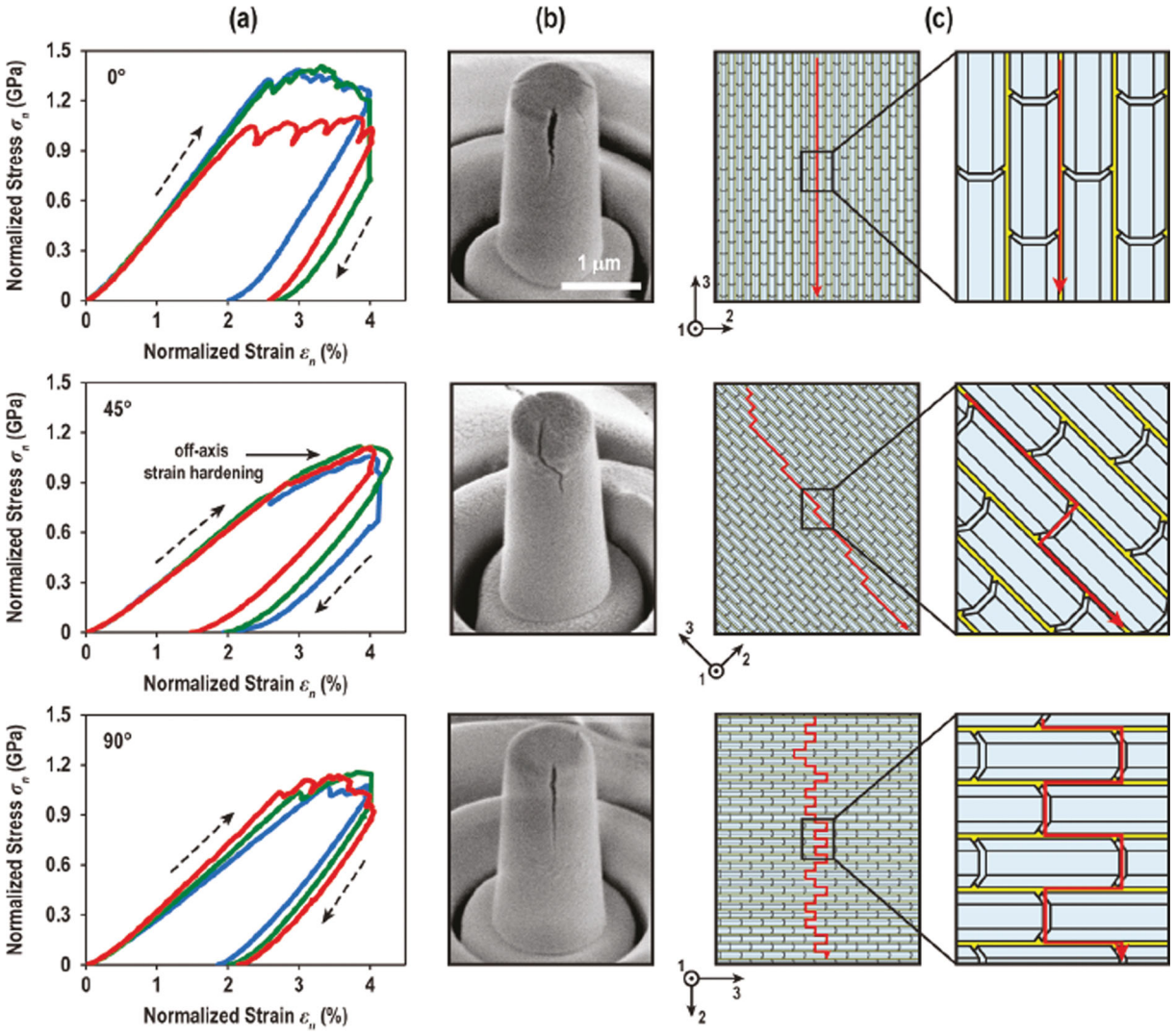

Figure 9. Anisotropic uniaxial compression behavior of ganoine micropillars at $\theta = 0°$, 45°, and 90° to its HAP rod axis (surface normal); (a) representative normalized engineering stress σ_n versus strain ε_n curves obtained from three individual micropillars for each θ, (b) typical crack propagation pathways observed via SEM after the compression (shown at a 45° stage tilt), (c) schematic of crack initiation and propagation mechanisms based on the ganoine nanostructure (reproduced with permission, Copyright 2011, American Chemical Society).[51]

strengths (~60 MPa) than in the 0° orientation (~40 MPa), as plotted in Figure 11c. Indeed, some in-plane anisotropy exists in both the cycloid and ctenoid scales, with orthogonal and double-twisted plywood patterns being reported. The plywood structure has been proposed to form a Bouligand arrangement;[45] this arrangement will be further discussed at the end of this section.

3.1.2. Osteoderms

Osteoderms are the counterpart of armor scales for reptiles (turtles, lizards, alligators) and mammals (armadillo). The order crocodilia contains notably crocodiles, alligators and caimans. All have osteoderms that cover the head, back and tail of the animal. The osteoderms on the backs of the alligators have massive bony plates with protrusions. One of them is shown in **Figure 12**a. These osteoderms have a surface characterized by a pattern of irregularities and have a central protrusion that is aligned with the back of the animal, forming dorsal ridges. The cross-sectional view shows that the bone contains dense structure close to outer surface and pores inside on two scales: the larger ones, with diameters of ~500 μm, and smaller ones, with diameters of ~100 μm (Figures 12b,c). Several large pipe-like channels can be seen (Figure 12b) and small channels, ~60 μm in diameter, are shown in Figure 12c.[35] The cross-section contains features which result from the alignment of collagen fibers (the dashed lines in Figures 12d-f, both in the compact region and around pores) to make up the bone; ligaments connect these fibers as shown in Figure 12f. A similar structure has been observed in polacanthid *Polacanthus foxii* and *Stegosaurus armatus*[53,54] (**Figure 13**). It contains cortical bone (which is dense) and primary lamellae and cancellous bone (which is porous). Some of the pipe-like vascular channels can also be observed (Figure 13b).[54]

Adv. Mater. **2012**,
DOI: 10.1002/adma.201202713

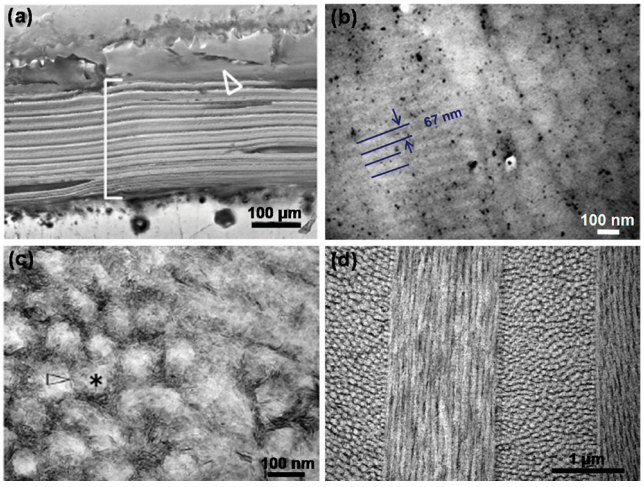

Figure 10. Different fish scales showing similar collagen-fiber lamellae; (a) cross-section of carp (*Cyprinus carpio*) scales (SEM) showing parallel collagen lamellae and external highly mineralized layer, (b) TEM of lamella parallel to fibers showing characteristic 67 nm pattern, (c) TEM of lamella perpendicular to collagen fibers showing fibrils with 100–200 nm diameter and interfibrillar mineral (from Figure 8b, 10c and 10d in Ref. [52], reproduced with permission, Copyright 2012, Elsevier), (d) TEM of the cross-section of *Pagrus major* scale showing co-aligned collagen fibers within each layer, which rotate alternately through an angle of ~90° (from Figure 4 in Ref. [46], reproduced with permission, Copyright 2003, Elsevier).

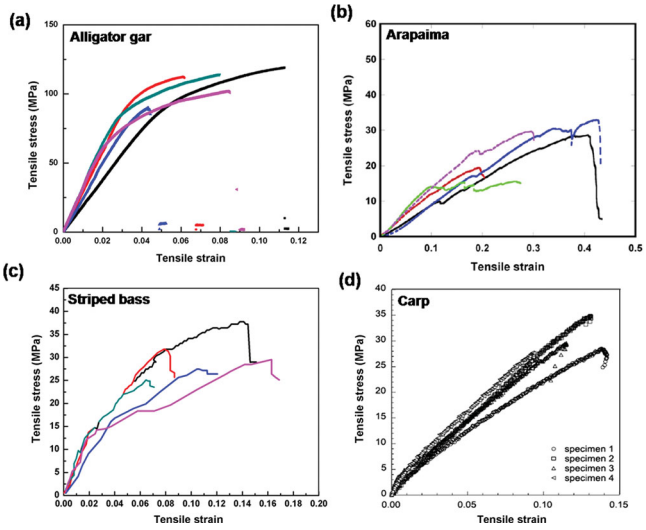

Figure 11. Comparison of the tensile response of (a) bone layer of a ganoid scale (alligator gar),[36] (b) a cosmoid scale (arapaima) (from Figure 13b in Ref. [43], reproduced with permission, 2011, Elsevier), (c) ctenoid scale (striped bass) (from Figure 3b in Ref. [25], reproduced with permission and (d) cycloid scale (carp) (from Figure 5b in Ref. [52], reproduced with permission, 2012, Elsevier). Each plot has the response of 4–5 specimens to show variation in mechanical response. The scales were all tested wet.

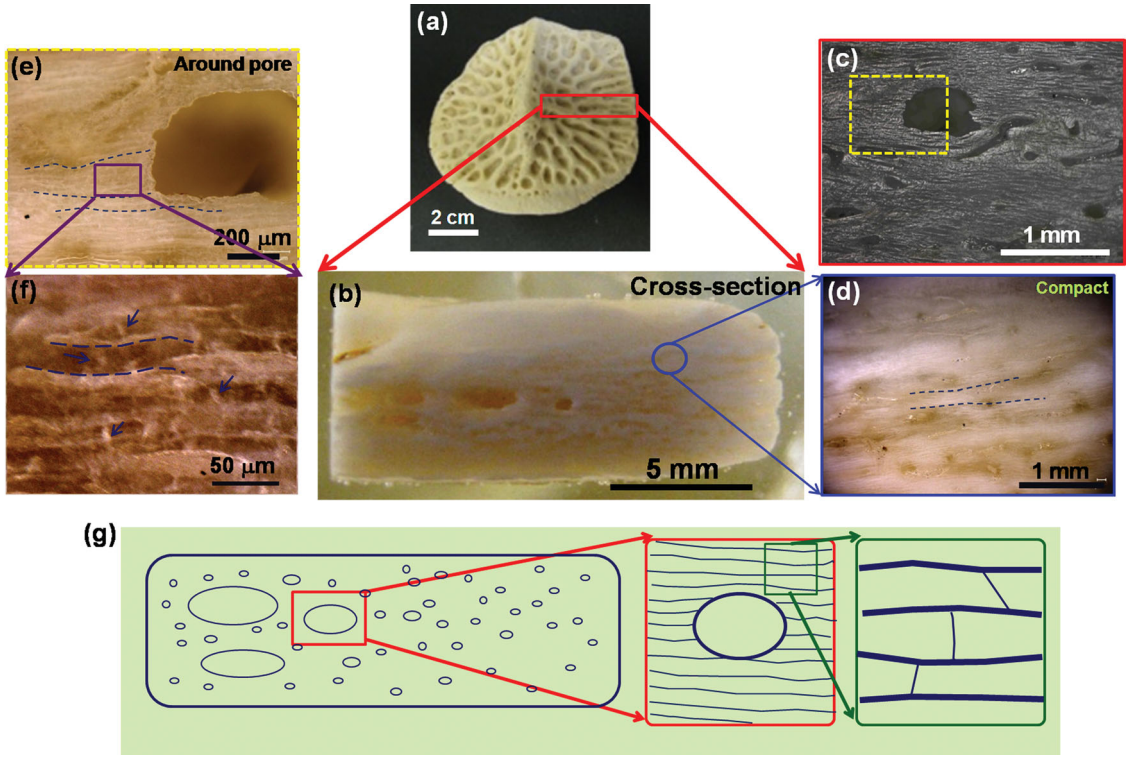

Figure 12. Structural characterization of the alligator osteoderm; (a) top view of one alligator scale, (b) cross-section view showing the porous structure, (c) voids in two scales, ~500 μm and a lamellae void with ~100 μm diameter, (d) relative compact part in the structure showing the fiber-like characteristic, (e) fibers tracing around a pore, (f) high magnification of the fiber-like characteristic showing the alignment of collagen fibers in the osteoderm with ligaments between them, (g) schematic drawing showing different elements of osteoderms.[35]

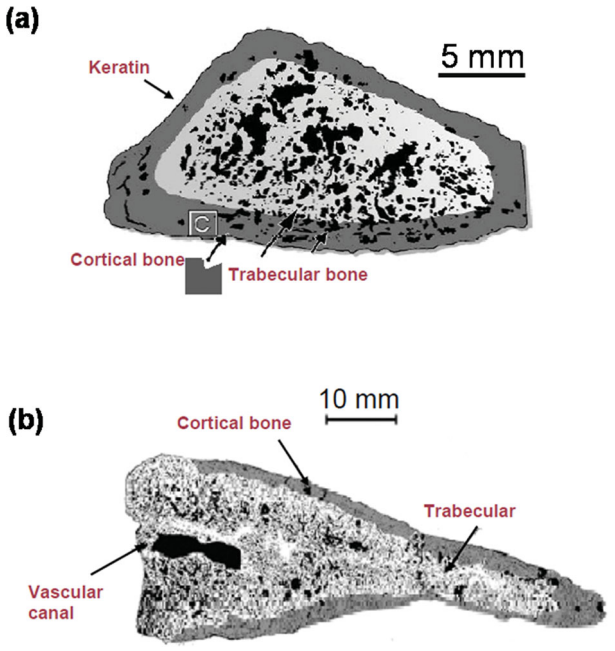

Figure 13. Cross-sections of selected osteoderms showing the similarities in the structure with the alligator osteoderms; (a) cross-section of a polacanthus *Polacanthis foxii* osteoderm (from Figure 3b in Ref. [53], reproduced with permission, Copyright 2004, Taylor & Francis), (b) cross-section of *Steogosaurus armatus* (from Figure 8b in Ref. [54], reproduced with permission, Copyright 2010, Springer).

The leatherback turtle also has osteoderms but the porosity is significantly larger than in the alligator. The leatherback turtle is unique among turtles in that the osteoderms are not covered with keratin but with skin. Another feature of the osteoderms is that they are not rigidly connected but allow considerable flexibility; in contrast to the alligator osteoderms, they are juxtaposed and are joined by sutures, as will be explained later. **Figure 14** shows such an osteoderm from one of the seven ridges that run along the turtle back (six out of seven ridges visible in Figure 1c).[35] The edges of the osteoderm are jagged and not smooth as those of the alligator. The cross-section shows the porosity which is distributed in voids of two sizes (similar to the alligator): 20–100 μm and 1–3 μm. The large voids are aligned in the plane of the osteoderm, with lamellae rings surrounding them. The sutures of the leatherback turtle osteoderms are shown in **Figure 15** and the zig-zag arrangement of the bone-adjoining osteoderms creates extrusions and intrusions that fit into each other.[34] This enables limited motion which has been measured to be roughly ±15°. This motion of the sutures is required for deep diving in which the lung cavity volume is reduced by the water pressure. Leatherback turtles are known to dive to depths greater than 1000 m corresponding to a pressure of ~10 MPa.

An assembly of plates from the plastron and two plates on the carapace ridge are shown in Figures 15a and 15b, respectively. The flexibility of their carapace enables the contraction of the body associated with the high hydrostatic pressures. Because of this, the sutures in the leatherback turtle are much

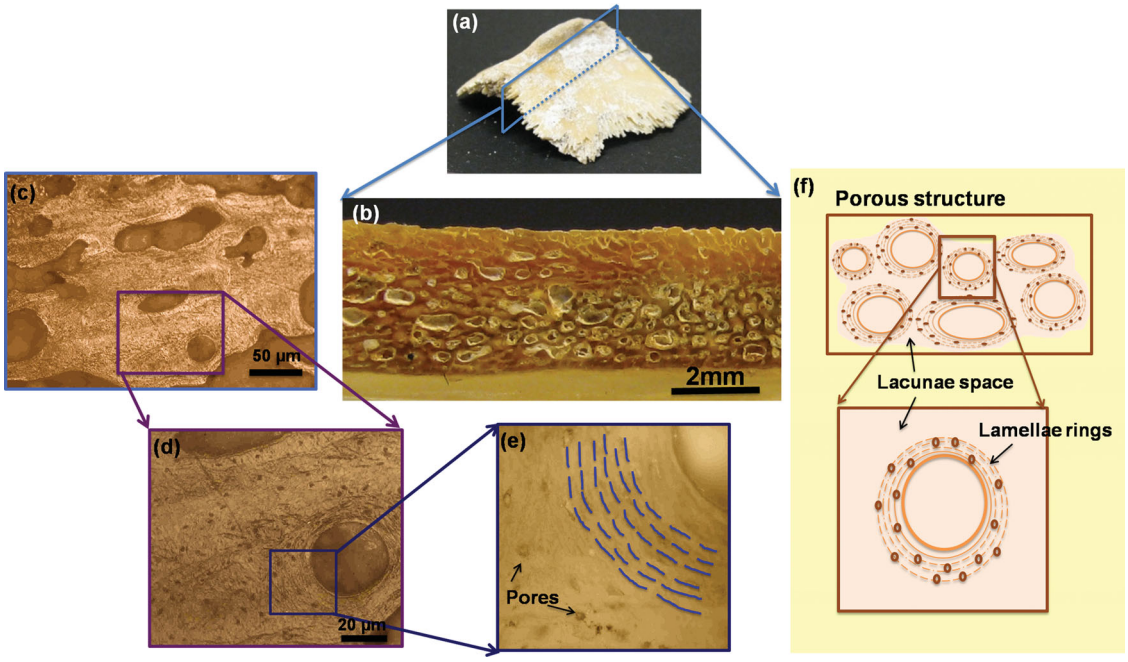

Figure 14. Osteoderm in the leatherback turtle; (a) side view from the ridge osteoderm, (b) longitudinal section showing the porous structure, (c) porosity showing alignment of voids, (d) lamellar rings and lacunae around pores, (e) lamellar rings and small pores, (f) schematic drawing of the structure.[35]

Adv. Mater. **2012**,
DOI: 10.1002/adma.201202713

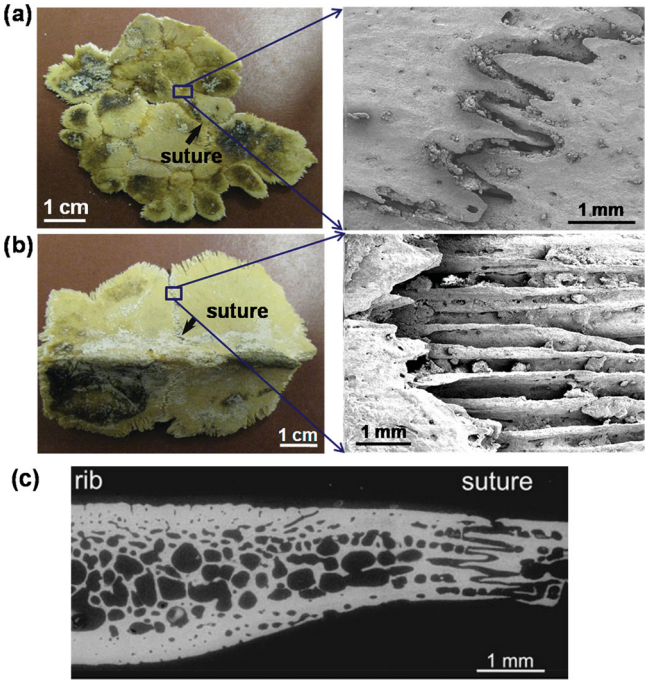

Figure 15. Structural characterizations of connections between armor units (from Figure 4 in Ref. [34], reproduced with permission, Copyright 2012, Springer); (a) suture between the ventral osteoderms of leatherback turtle, (b) suture between the dorsal osteoderms of leatherback turtle, (c) side view of suture in red eared turtle (from Figure 1 in Ref. [55], reproduced with permission).

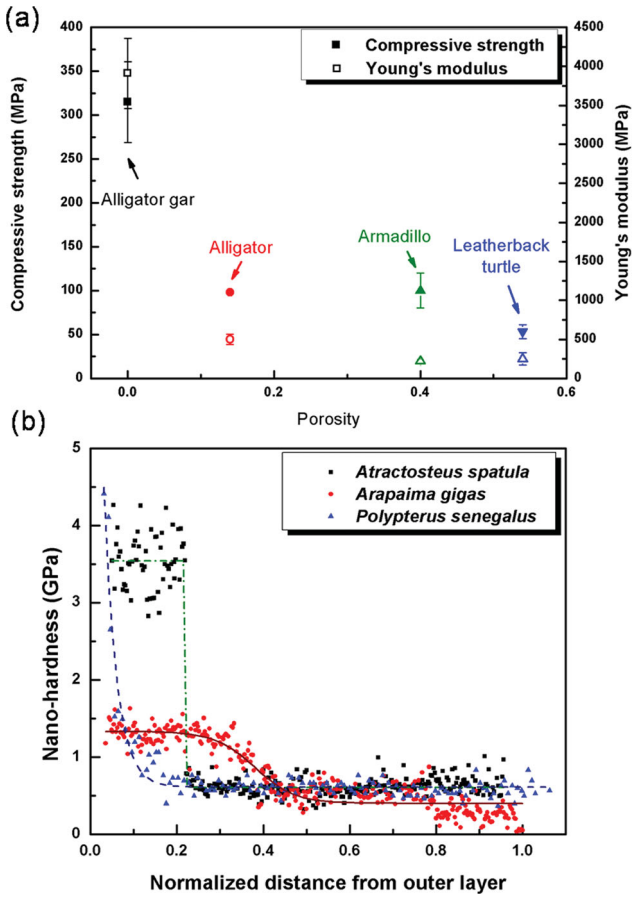

Figure 16. Comparison of mechanical properties between different natural dermal armors; (a) comparison of strengths and Young's moduli of fish (alligator gar) scales and reptile (alligator and leatherback turtle) osteoderms in compression, (b) hardness as a distance from the surface for three fish scales (nanohardness data of *Polypterus senegalus* scale was obtained from Ref. [19], reproduced with permission, Copyright 2008, Nature Publishing Group).

less rigid than in other turtle species. Figure 15c shows the lateral view of a suture in a Red Eared Turtle, as researched by Krauss et al.[55] The closeness of the intrusions and extrusions suggests a smaller maximum angle of bending between the plates. Indeed, this angle was measured to vary between 0.8° and 1.7°, in comparison with the leatherback turtle, where it was estimated to be 15°. Similarly, the suture joints in units having both triangular and rectangular geometries have been analyzed by Li et al.,[56] who established their stiffness and how the load was transmitted into the skeletal weight. The results obtained have relevance to biomimetic design of flexible dermal armor.

The mechanical properties of bony scales and osteoderms are dependent on the degree of porosity, which increases progressively from the alligator gar, alligator, armadillo, to leatherback turtle. Specifically, both the Young's modulus and the compressive strength scale with decreasing porosity (**Figure 16**a).

The hardness of the fish scales, conversely, is more often highly non-uniform, with a harder, more highly mineralized layer on the surface. This can be seen in Figure 16b where the hardness variation across the cross-section of two ganoid and one cosmoid scale is shown. Note how the hardness of ganoine is much higher than the one in the outer layer of the arapaima scale by virtue of its different structure and mineral content.

3.2. Fracture Mechanisms: Crack Propagation and Structural Failure

3.2.1. Alligator Gar Scale

A necessary property of dermal armor is fracture toughness, which represents its resistance to flaw-like damage and the consequent unstable propagation of cracks. Alligator gar scale derives its toughness in part from its inner bony layer, which influences the path of the crack by causing it to interfere with its structure. Quantitative evaluation of the fracture toughness of alligator gar as a function of crack extension (i.e., the R-curve[57]) is shown in **Figure 17**,[36] based on measurements of the three-point bending of notched beams within the environmental scanning electron microscope (Figure 17).[36] The toughness of alligator gar scale is comparable to that of other mineralized tissues such as bone and teeth; however, the microstructure, comprising tubules roughly 2 to 5 μm in diameter, plays an interesting role in affecting the fracture resistance under dry versus wet conditions. With the scale fully hydrated

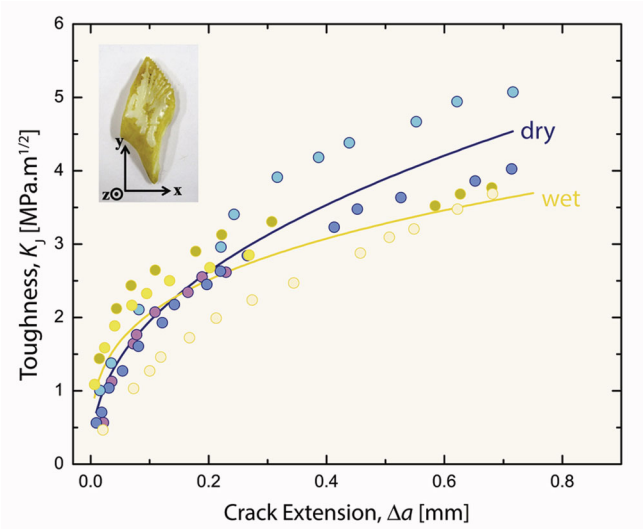

Figure 17. Fracture toughness crack-resistance curves (R-curves) showing resistance to fracture in terms of the stress intensity, K_J, as a function of crack extension, Δa, for dry and wet alligator gar scales. Three-point bending samples were prepared such that the crack propagated in the *x*-direction (see inset) and tested in an environmental scanning electron microscope (ESEM).[36]

in water, cracks in the alligator gar scales follow a roughly linear path[36] (**Figure 18**a), whereas once the scale becomes dry, cracks follow a trajectory where they are attracted to the tubules

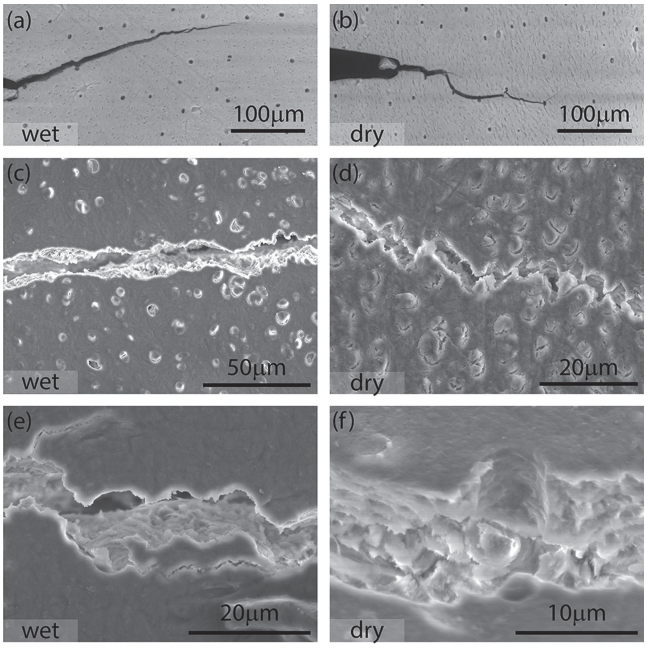

Figure 18. Cracking paths of alligator gar scale tested in wet and dry conditions;[36] (a) sample tested in wet condition showing a straight crack propagation, (b) sample tested in dry condition showing the crack going through the tubules, (c) minor crack deviations caused by the tubules and collagen fibers, (d) significant meandering of cracks through tubules and collagen fibers, (e) crack preferentially propagating around both tubules and collagen fibers in wet scale, (f) crack penetrating interface between collagen fiber and matrix in dry scale.

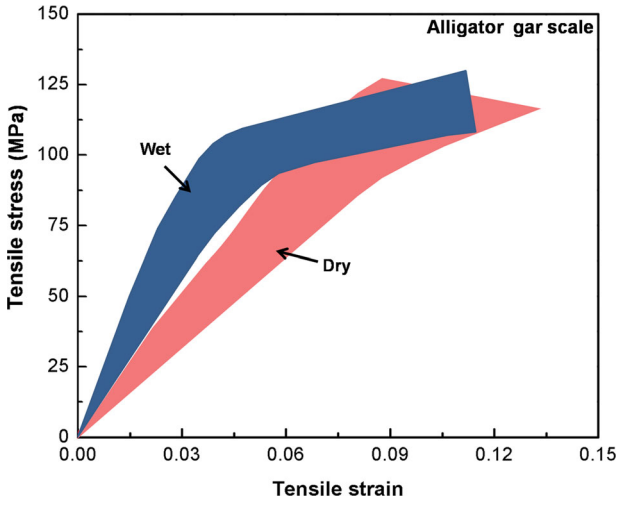

Figure 19. Range of tensile stress-strain curves of wet (5 specimens) and dry (18 specimens) alligator gar scales represented by bands. Note the bi-linear response of wet specimens that is clearly distinguishable from linear response of dry specimens which lack evidence of plastic deformation.[36]

causing a deflected and twisted crack path (Figure 18b). Cracks in general are attracted to voids; specifically they follow a low modulus phase, and the tortuosity created by such crack paths can increase the fracture toughness extrinsically[58] by a factor of up to 2 by in-plane deflections and even up to 6 if crack twisting is involved. Similar behavior is seen in tooth dentin where the crack again follows the dentinal tubules (provided they are not filled with mineral as in aged dentin).[59] However, under more physically realistic wet conditions, the crack path appears to be unaffected by the presence of the tubules (Figure 18c) or other smaller features, such as collagen fibers (Figure 18e), all of which provide a source of extrinsic toughening under dry conditions by causing the crack to meander (Figures 18d,f). However, to counter this reduction in extrinsic toughness, wet alligator gar scales display far more post-yield deformation.[34] **Figure 19** shows the range of stress-strain tensile curves for wet and dry scales. The bi-linear response for wet scale contrasts with the linear response of dry scales. The resulting "plasticity" in the wet material, caused by hydrogen bonding between the collagen and water molecules, enhances the intrinsic toughness by increasing ductility. Consequently, the difference in toughness between wet and dry scales is not that large and only becomes apparent as the crack extends (Figure 17) where the extrinsic toughening mechanisms become more active.

3.2.2. Arapaima Scale

The unique structure of the arapaima scale is composed of inner layers of mineralized collagen fibrils arranged in lamellae forming a Bouligand pattern[45] and a highly mineralized outer layer that both provide mechanisms to dissipate energy during fracture. Tensile tests of notched arapaima scales show how some individual layers of collagen fibers fracture, while others remain intact[60] (**Figure 20**); this represents a potent form of crack bridging, another extrinsic toughening mechanism, which is prevalent in many cross-ply fiber-reinforced plastics.

Adv. Mater. **2012**,
DOI: 10.1002/adma.201202713

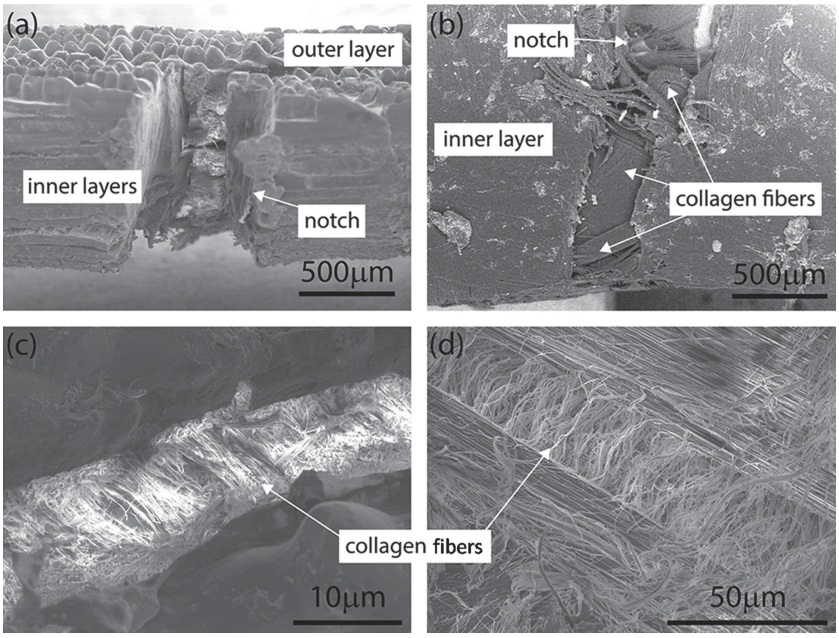

Figure 20. Failure of structural layers in notched arapaima scale samples; (a) top view showing cross-section of the notched samples after tests, (b) the notch tip with stretched and distorted collagen fibers pulled out by crack propagation, (c) optimally aligned fibers carrying a larger portion of the tensile load, (d) stretched or broken collagen fibers in different orientations.[60]

In this regard, biological materials are most resistant to tensile stresses when the collagen fibers are oriented parallel to the maximum tensile stress due to the fiber's substructure, which is composed of an array of collagen fibrils embedded with oriented mineral crystals. As the lamellae that are misaligned in the arapaima scale split along the fibers, the more optimally aligned fibrils carry a larger portion of the load. Additionally, collagen fibrils span the divide between the broken and intact layers, providing resistance to the deformation.

3.3. Strategies for Dermal Armor to Provide Flexibility

Three strategies which are used in nature to connect rigid elements for armor are depicted schematically in **Figure 21**.[34] In the armadillo carapace, the elements are hexagonal in the pectoral part, with elastic Sharpey's fibers (collagen fibers) connecting to the adjoining osteoderms. In the alligator gar and Senegal bichir, the bony scales have some overlap and the exposed (non-overlapped) regions are covered with ganoine. In the leatherback turtle, sutures forming a zig-zag pattern ensure a minimum of non-bone area and create great stiffness and flexibility. Sharpey's fibers are also found between bone plates in the osteoderms of other animals. For example, the cranial vault and facial skeleton contain Sharpey's fibers as structural connections.[61] The Sharpey's fibers, oriented perpendicular to the edges of the tiles, provide flexibility to the armadillo, as shown schematically in Figure 21. Collagen fibers also act as junction between fish scales. However, the fish scales do not arrange in a juxtaposed style, but instead are overlapped. The collagen fibers are located between the scales in the overlap portion and at the edges of the scales to connect them together to form rows. The "line-junction" at the edges of fish scales also connects them to adjacent rows of fish scales. Hence, a part of the bony component of scales is hidden below the other scales, only leaving the ganoine apparent in the case of the *Polypterus senegalus*[19] and *Atractosteus spatula*.[28,34] The connection and overlap mechanisms for these ganoid scales are shown in Figure 21.

The leatherback turtle shell has yet a different joining strategy, consisting of intrusions and extrusions in a jagged geometry (Figure 21). Indeed, this strategy is common to all turtles.[56] The plates in the plastron (belly plate) are smaller than those on the carapace (Figure 15). These junctions, called sutures, are effective, but have less flexibility than the fish scales and armadillo osteoderms. It is for this reason that the turtle cannot bend its body as effectively as fish. In contrast with the armadillo and fish armor, the osteoderms of the leatherback turtle are irregular and rely on the sutures to connect to each other (Figures 1,15). Leatherback turtles can dive to great depths and the suture connection mechanism provides more stiffness and less flexibility compared to the mechanism (Sharpey's fibers) of armadillo armor. However, it provides much greater flexibility than other turtles which are covered with a rigid keratin carapace.

4. Protection by Fish Scales Against Predation

Protective scales on fish in general provide effective protection against fish bites. This has been the focus of several

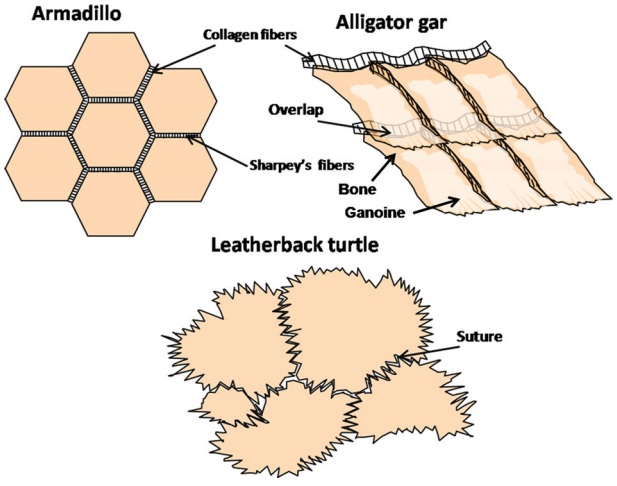

Figure 21. Three different strategies to provide flexibility: collagen fibers connecting juxtaposed hexagonal osteoderms in armadillo; overlap between bony scales in alligator gar; suture between osteoderms in leatherback turtle plastron (from Figure 3 in Ref. [34], reproduced with permission, Copyright 2012, Springer).

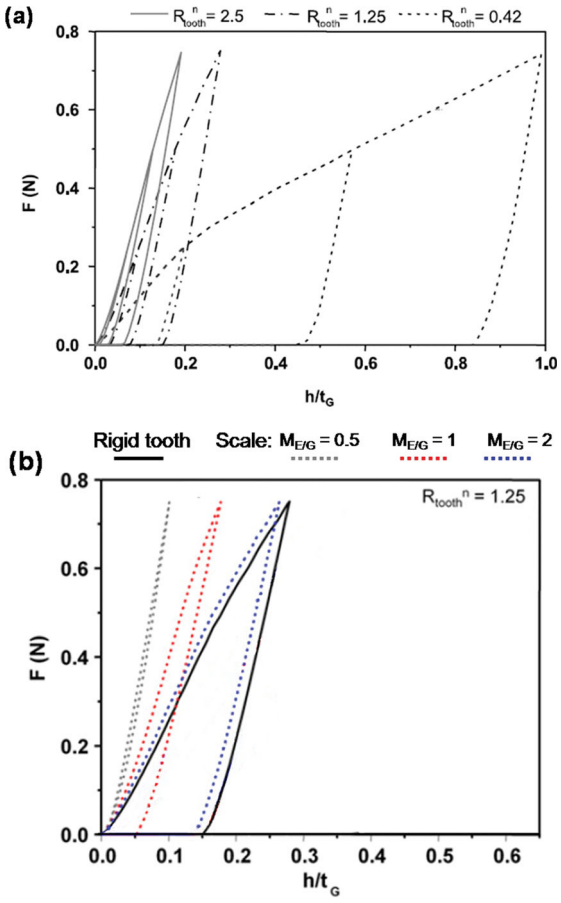

Figure 22. Finite element calculations of penetration of *Polypterus senegalus* scale by simulated Polypterus tooth; (a) effect of variation of normalized tooth tip radius (R^n_{tooth} = 2.5, 1.25, 0.42) on the normalized penetration as a function of load. As tooth becomes sharper (smaller R^n_{tooth}) penetration increases, (b) effect of tooth stiffness on load vs. normalized penetration. Penetration is the largest for rigid tooth and decreases for decreasing stiffness (taken from Figure 4a and Figure 7a in Ref. 32; Reproduced with permission.[32] Copyright 2011, Elsevier).

recent studies, on the ganoid scales of the Senegal bichir,[32] ctenoid scales of the striped bass.[25] and cosmoid scales of the arapaima.[44]

For the analysis of the Senegal bichir where intraspecies predation is the principal threat, Song et al.[32] conducted a finite element analysis (FEA) of the ganoid scales where they varied tooth and scale parameters and established what effects this had on the mechanical response. Specifically, they varied the radius of curvature in the tooth tip, the enameloid layer thickness and hardness, as well as the ganoine thickness and hardness in the ganoid scale. **Figure 22**a shows that the tooth tip radius R (sharpness of the tooth) has a significant effect on the penetration; for an identical load of 0.6 N, the penetration for a normalized root radius of R^n = 0.42 (R = 5 μm) is over five times that for R^n = 2.5 (R = 30 μm). The experimentally measured values for real bichir teeth vary between R = 5 and 30 μm, with a half-angle at the tip of 22°. So, as the root radius decreases, i.e., the tooth becomes sharper, the penetration depth increases at a specified load.

Figure 22b shows the effect of the mechanical strength of the tooth on the normalized penetration, h/t_G (penetration depth h normalized by the ganoine thickness, t_G). The force-depth curve relating to a perfectly rigid tooth is the black solid line (on the right); the relative mechanical strength of the tooth (assumed to be uniformly enameloid without a dentine core), $M_{E/G}$, defined as the ratio of the Young moduli (assumed to be the same as the strength ratio) between the enameloid and the ganoine, is indicated at the top of Figure 22b; this ratio varies between 0.5 and 2.0. These results indicate, predictably, that the more deformable the tooth, the smaller the penetration on the scale at the same load.

Zhu et al.[25] penetrated the scale of striped sea bass *(Morone saxatilis*) with a sharp indenter. The scale was laid on a soft silicone substrate having properties similar to flesh. They used a steel indenter with a tip radius of 25 μm, *i.e.*, similar to that used in the simulations by Song et al.[32] and close to actual measurements on piranha.[44] They used the scale both with and without the slightly mineralized surface layer (bony layer) and found that the external layer had an important effect, doubling the penetration resistance from that of the inner collagen layer. The characteristic response, together with the schematic drawings and micrographs of the surface deformation during the penetration procedure, are shown in **Figure 23**. The entire penetration procedure can be divided into three stages with progressively increasing penetration depth: the first stage is essentially elastic loading which terminates with cracking of the 'bony' layer, Stage II involves the penetration of collagen, while in Stage III the tip of the indenter has already traversed the scale. The measured maximum force, 3 N, is consistent with the calculations of Song et al.[32]

The analysis of scales and the evaluation of the distribution of stresses under them when they are subjected to compression have been carried out by Vernerey and Barthelat.[62] They concluded that this strain-stiffening mechanism in fish-scale structures is a characteristic shared by a large number of biological structures and materials and is a strategy to prevent structural damage and failure, as shown schematically in **Figure 24**. The penetration of a sharp object is significantly affected by the presence of scales which adjust themselves to the load and redistribute the stresses in the proximity of the surface. The scales redistribute the concentrated load by the indenter over a larger area. Whereas the indentation is deep and narrow for an unprotected surface, it becomes wider and shallower in the presence of scales.

Vernerey and Barthelat[62] varied several parameters, in particular the ratio K^d/EI (EI is bending resistance, K^d is stiffness or attachment resistance) and the scale density $\lambda = 1/d$ (defined as the average number of overlapping scales in a cross-section of the skin), and showed that scale design, arrangement and properties can be tailored to achieve a wide spectrum of responses; Figure 24b demonstrates the effects of these parameters on penetration variables.

The principal predator of the arapaima is the piranha, which was the basis of a study by Meyers et al.[44] using real indenters (piranha teeth) directly impinging on scales. The teeth of the piranha fish are very sharp, with a radius at the tip of ~14 μm

Adv. Mater. **2012**,
DOI: 10.1002/adma.201202713

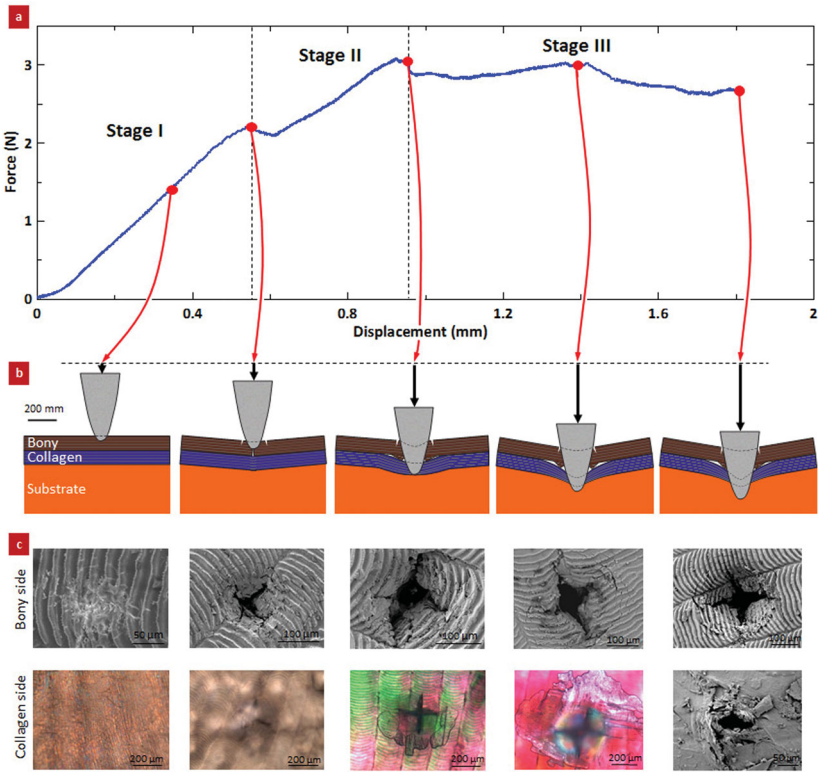

Figure 23. Deformation of the bass scale during a puncture test; (a) Load- displacement curve of the penetration of striped bass scale by a sharp needle simulating tooth (R_{tip} = 25 µm). The resulting curve is divided into three stages corresponding to Stage I - elastic deflection of sale; Stage II - fracture of mineralized layer and, Stage III - penetration of collagen lamellae and formation of triangular (flaps), (b) schematic drawing showing how the structure damaged by the load during the test, (c) Deformations (top-view) of the scale during the puncture test (from Figure 5 in Ref. 25). Reproduced with permission.[25]

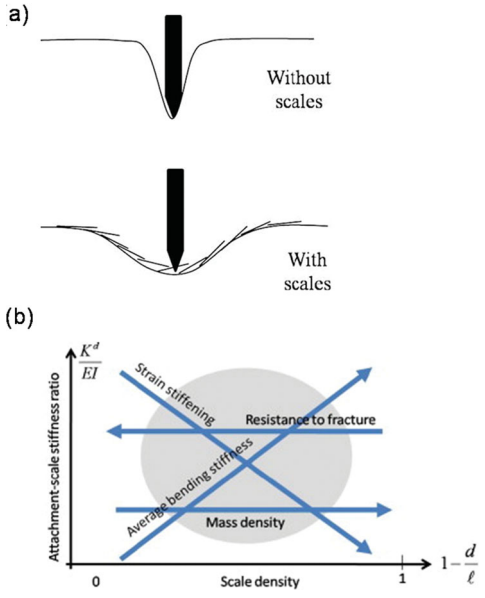

Figure 24. (a) Illustration of the role of fish scales in preventing unstable localized deformation; (b) effect of attachment/stiffness ratio of scales (k^d/EI) and density on various parameters (from Figures 6 and 7 in Ref. [62], reproduced with permission, Copyright 2010, Elsevier). (k^d is the angular stiffness of the attachment of the scale and EI is the bending stiffness of the scale).

and a semi-angle of ~20° (across the thickness), similar to the Senegal bichir. The calculated force for the piranha studied (an average sized red piranha, the most predatory species, *Pygocentrus natteri*) was 17 N.[44]

The sharp piranha tooth, shown in **Figure 25**a,[34] has an angle of ~60° (in the plane of the tooth), with clear serrations visible on the edge of the tooth (right hand, below). The microhardness of the enamelous portion of the piranha tooth is ~1.5 GPa which is higher than that of the mineralized surface of the arapaima scale (~0.7 GPa measured by nanohardness testing). It is presumed that this sharp tooth with serrations on the edge can compress the scales to form an indentation. To ascertain this, mechanical tests were performed with the tooth attached to the crosshead and forced onto the external surface of the arapaima scales. This experiment showed how successful the armor scales can be as the tooth failed on the indentation; these events are marked by arrows on the force-displacement curves and correspond to load drops. Figure 25b shows the broken tooth after penetration (right hand). Even though it had twice the hardness of the scales, it appears that the tooth broke either during penetration or in the extraction process.[34]

Figure 26 and 27 show the surface of the scale after indentation with a piranha tooth. Two regions were penetrated: the covered layer, characterized by a regular pattern of ridges with ~0.3 mm (Figure 26) and the exposed part, which has a thicker mineral layer (Figure 27). The tooth penetrates into the covered part of the scale, eventually exposing the collagenous lamellae and perforating them. Cracks in the mineralized surface layer enable observation in the lamellae; these are marked by arrows in Figure 26a. The collagen fibers that are deformed, stretched and eventually fractured under tension are shown in Figures 26b–d; arrows show broken fibers in Figure 26c. The exposed part of the scale provides greater resistance to penetration that can lead to tooth fracture. A fractured embedded tooth is shown in Figure 27a. This mineral layer is more effective against the penetration due to its greater hardness. At the sharp edge of the tooth one can see stretched collagen fibers. These fibers eventually fracture, as shown in the detailed view of Figures 27b–d.

5. A Singularity in Flexible Natural Armor: the Pangolin

An unusual armor is found on the pangolin, a small insectivore that lives in the rain forests of Asia and Africa. It ranges from 0.4–1 m in length and weighs up to 18 kg. The exterior of the animal is covered with non-mineralized keratin scales, shown

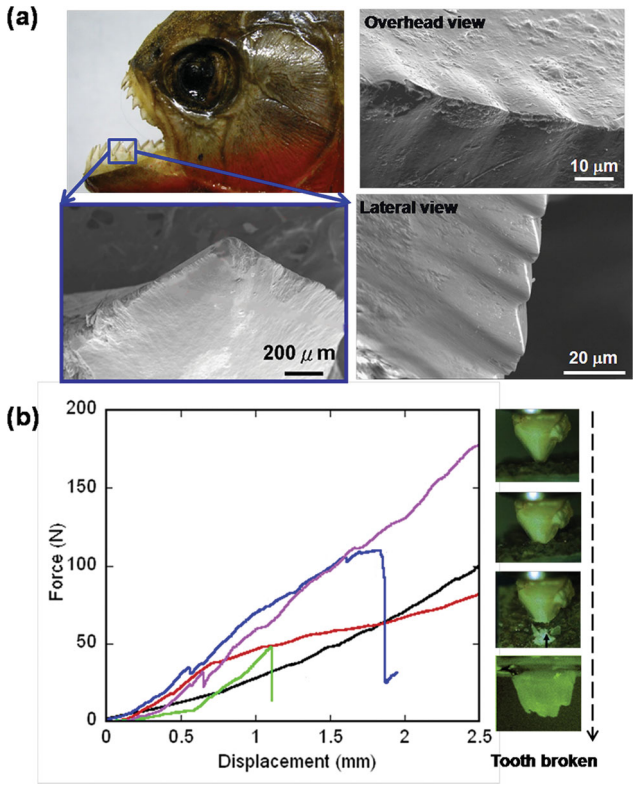

Figure 25. Piranha teeth and their puncturing effect on arapaima scale; (a) the red piranha and details of its teeth showing serrations; (b) force-penetration by the piranha tooth through the external region of arapaima scale. Note the load drops corresponding to fracture of teeth before full penetration (~2 mm) is accomplished. The broken tooth is shown in lower right-hand corner (from Figure 9 in Ref. 34. Reproduced with permssion.[34] Copyright 2012, Springer).

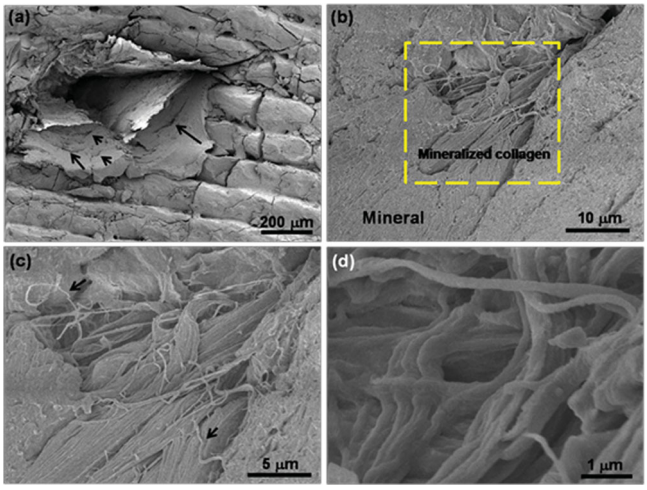

Figure 26. Penetration into covered portion of arapaima scale by the piranha tooth; (a) the whole indentation, arrows showing cracks on the mineral layer around the indentation, (b) mineralized collagen fibers in the exposed area penetrated by tooth, (c) mineralized collagen fibers, arrows showing the fractured curled fibers, (d) collagen fibers in different orientations.

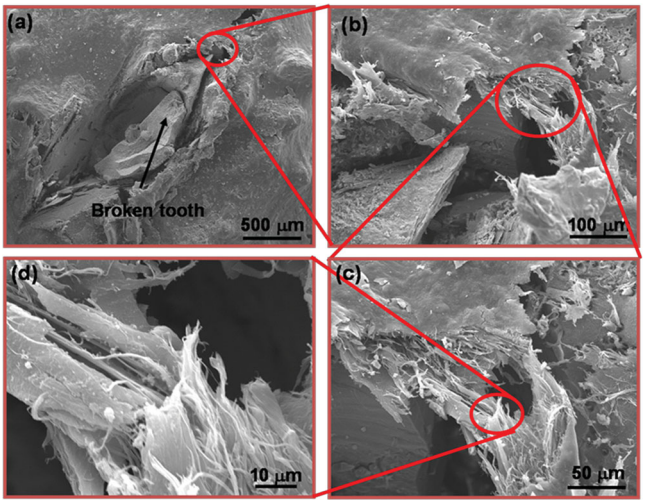

Figure 27. Penetration into the exposed part of arapaima scale by the piranha tooth; (a) the whole indentation with broken piranha tooth, (b) and (c) collagen fibers stretched out at the sharp edge of indentation, (d) some fractured collagen fibers.

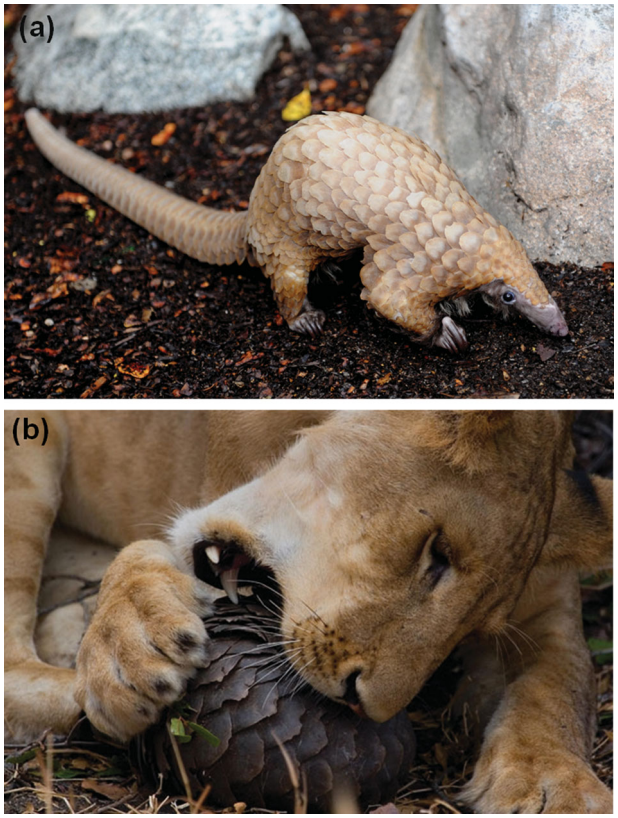

Figure 28. Protection of the keratinous pangolin armor; (a) the scales overlapping on the pangolin body, photograph by B.Y. Zhang (b) a lion unsuccessfully trying to defeat a pangolin dermal armor; she finally gave up. Reproduced with permission.[63] Copyright, Mark Sheridan-Johnson.

Adv. Mater. **2012**,
DOI: 10.1002/adma.201202713

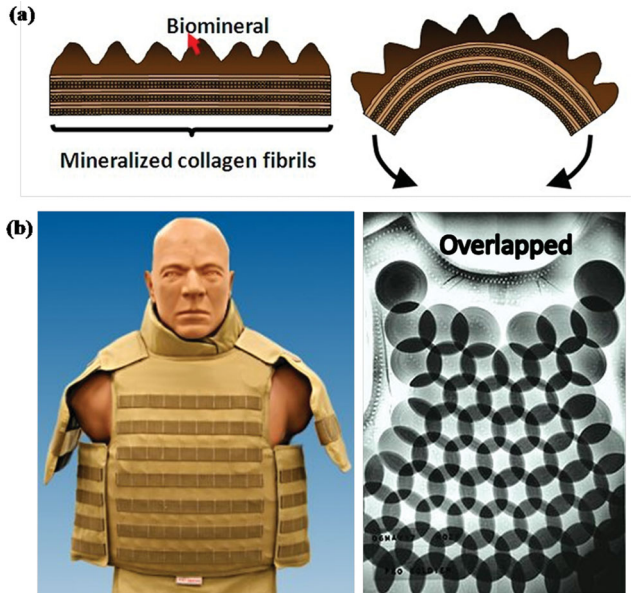

Figure 29. Bioinspired flexible dermal armor; (a) conceptual view of flexible ceramic using arapaima scales as bioinspiration (Reproduced with permission.[44]); corrugations in ceramic decrease deleterious effects of tensile stresses; and (b) Dragon Skin® armor Reproduced with permission.[64] Copyright, Murray Neal & North American Development Group LLC.

in **Figure 28**a, which weigh up to 20% of the entire animal. When curled up, these scales extend from the body producing a barrier of razor-sharp edges and are a formidable defense (Figure 28b).[63] It has been reported that a pride of lions toyed with a balled-up pangolin for several hours before giving up. The edges of the keratin scales are also sharp and can cut a potential predator.

6. Bioinspiration from Natural Armor

The principle underlying such natural armor is that the overlapping scales can resist the attack from teeth, with the junction between the scales providing flexibility. A prime example is the arapaima scale, which consists of a foundation of collagen arranged in successive layers with different orientations of the fibers (Figures 3a and 6) that support a highly mineralized external layer, which itself has ridges to minimize the effects of tensile stresses produced by flexing. A conceptual view of such a "flexible" ceramic is shown in **Figure 29**a; upon bending, the tensile stresses are limited to the bottoms of the ridges. We believe that these simple concepts can serve as inspiration for synthetic armor designs.

Another concept that has been used since antiquity is scale armor. In scale armor, the individual elements are sewn or laced to a backing and form overlapping rows resembling the scales of a fish/reptile. This armor was used by Scitian, Roman, Bizantine, and Japanese warriors. Examples are the Lorica squamata (squamata is the scientific word for scaled reptile), a Roman scale armor and gyorin kozane, the Japanese equivalent. "Dragon Skin" armor (Figure 29b) uses a design principle similar to the scale armor, although it was not inspired by fish scales. Dragon Skin consists of overlapped discs of silicon carbide ceramic. The overlapped discs provide a range of motion which makes the Dragon Skin armor highly flexible; the overlapped hard discs are designed to resist bullet penetration. This battlefield proven technology is still under development for the military 20 mm and 25 mm projectile threats.

7. Conclusions

Different species have evolved flexible and hard dermal armor, which is now inspiring researchers to produce synthetic systems based on similar concepts. As pointed out by the systematic investigations of Fratzl and Weinkamer,[65] the structures in nature are not only hierarchical but multifunctional as well. In the case of dermal armor, other important functions are coloration, hydrodynamic flow, temperature and fluid regulation. These dermal armors have developed independently in fish, reptiles, and mammals. This independent evolution process is known as 'convergent evolution'.

The flexible dermal armor of fish possesses a hierarchical structure consisting of a more compliant foundation and a harder surface layer. In mammals and reptiles, the protection is offered by osteoderms, which are joined by collagen fibers called Sharpey's fibers or sutures. In fish, protection is offered by scales, which connect to each other with significant overlap and to the body. An important function of this flexible dermal armor is to distribute the load applied locally (by, for instance, teeth) to a larger region, thus decreasing stress concentration and damage to the underlying tissue. Therefore, flexible armor is a compromise between protection and mobility, and different species have developed combinations of these best suited for survival and success. In the case of the leatherback turtle, the flexibility is significantly lower than in fish because the propulsion is accomplished by paddle feet; however, it is considerably higher than other turtles and tortoises.

The flexible scales of the arapaima can serve as inspiration for flexible ceramics, with numerous potential applications. One connection method between scales, by overlapping, is already commercially available and incorporated into Dragon Skin armor. Another connection method between osteoderms, by sutures, also has relevance to the biomimetic design of flexible dermal armor due to their load transmission mechanisms.[56]

Acknowledgements

This work is supported by the National Science Foundation, Ceramics Program Grant (DMR-1006931) and the University of California Lab Research Program (09-LR-06-118456-MEYM). The involvement of ROR was supported by the Director, Office of Science, Office of Basic Energy Sciences, Division of Materials Sciences and Engineering, of the U.S. Department of Energy under Contract No. DE-AC02-05CH11231. We are grateful to Dianne Ulery and Gaspar Ritter of Kuryala Lodge (Araguaia River) for providing scale specimens of alligator gar and arapaima,

respectively. Mr. Steve Lee skillfully drew Figure 3. We thank B.Y. Zhang for taking the picture of the pangolin.

Received: July 5, 2012
Published online:

[1] http://ironshots.smugmug.com/keyword/museum%20of%20nature%20and%20science/1/92036125RK8Q8#!i=92036125&k=RK8Q8
[2] http://digitalmedia.fws.gov/cdm4/item_viewer.php?CISOROOT=/natdiglib&CISOPTR=401&CISOBOX=1&REC=2 (accessed October 2012)
[3] http://www.tnaqua.org/OurAnimals/Fishes/Arapaima.aspx (accessed October 2012)
[4] K. Curry Rogers, M. D'Emic, R. Rogers, M. Vickaryous, A. Cagan, *Nat Commun.* **2011**, *29*, 564.
[5] S. F. Gilbert, G. A. Loredo, A. Brukman, A. C. Burke, *Evol. Dev.* **2001**, *3*, 47.
[6] J. Cebra-Thomas, F. Tan, S. Sistla, E. Estes, G. Bender, C. Kim, P. Riccio, S. F. Gilbert, *J. Exp. Zool. Part B* **2005**, *304B*, 558.
[7] W. G. Joyce, S. G. Lucas, T. M. Scheyer, A. B. Heckert, A. P. Hunt, *Proc. R. Soc. B* **2009**, *276*, 507.
[8] M. K. Vickaryous, B. K. Hall, *J. Morph.* **2006**, *267*, 1273.
[9] I. H. Chen, J. H. Kiang, V. Correa, M. I. Lopez, P.-Y. Chen, J. McKittrick, M. A. Meyers, *J. Mech. Behav. Biomed. Mater.* **2011**, *4*, 713.
[10] M. R. Seidel, *Herpetologica* **1979**, *35*, 375.
[11] J. D. Currey, *J. Mech. Behav. Biomed. Mater.* **2010**, *3*, 357.
[12] L. Zylberberg, J. Castanet, *J. Morphol.* **1985**, *186*, 327.
[13] C. Chang, P. Wu, R. E. Baker, P. Maini, L. Alibardi, C.-M. Chuong, *Int. J. Dev. Biol.* **2009**, *53*, 813.
[14] M. K. Vickaryous, J.-Y. Sire, *J. Anat.* **2009**, *214*, 441.
[15] R. I. C. Spearman, *Zool. J. Linn. Soc. - Lond.* **1967**, *46*, 267.
[16] J. McKittrick, P.-Y. Chen, S. G. Bodde, W. Yang, E. E. Novitskaya, M. A. Meyers, *JOM* **2012**, *64*, 449.
[17] E. S. Goodrich, *Proc. Zool. Soc. Lond.* **1907**, *77*, 751.
[18] J.-Y. Sire, A. Huysseune, *Biol. Rev.* **2003**, *78*, 219.
[19] B. J. F. Bruet, J. H. Song, M. C. Boyce, C. Ortiz, *Nature* **2008**, *7*, 748.
[20] T. Ørvig, *Arkiv Zool.* **1957**, *10*, 367.
[21] G. H. Roux, *S. Afr. J. Med. Sci.* **1942**, *7*, *(Biol. Suppl.)*, 1.
[22] M. M. Smith, M. H. Hobdell, W. A. Miller, *J. Zool. Lond.* **1972**, *167*, 501.
[23] H. Onozato, N. Watabe, *Cell Tissue Res.* **1979**, *201*, 409.
[24] A. Bigi, M. Burghammer, R. Falconi, M. H. J. Koch, S. Panzavolta, C. Riekel, *J. Struct. Biol.* **2001**, *136 (2)*, 137.
[25] D. Zhu, C. F. Ortega, R. Motamedi, L. Szewciw, F. Vernerey, F. Barthelat, *Adv. Eng. Mater.* **2011**, *13*, B1.
[26] http://australianmuseum.net.au/Placoid-scales/ (accessed October 2012, Sue Lindsey © Australian Museum)
[27] W. Raschi, C. Tabit, *Aust. J. Mar. Freshwater Res.* **1992**, *43*, 123.
[28] P. Y. Chen, J. Schirer, A. Simpson, R. Nay, Y.-S. Lin, W. Yang, M. I. Lopez, J. N. Li, E. A. Olevsky, M. A. Meyers, *J. Mater. Res.* **2012**, *27*, 100.
[29] J.-Y. Sire, *Amer. J. Anat.* **1989**, *186*, 315.
[30] Z. Vokac, N. E. D. Ahmed, A. M. A. Magid, *J. Exp. Biol.* **1972**, *57*, 461.
[31] K. D. Jandt, *Nat. Mater.* **2008**, *7*, 692.
[32] J. Song, C. Ortiz, M. C. Boyce, *J. Mech. Behav. Biomed. Mater.* **2011** *4*, 699.
[33] K. Curry Rogers, M. D'Emic, *Sci. Am.* **2012**, *306*, 48.
[34] W. Yang, I. H. Chen, J. McKittrick, M. A. Meyers, *JOM* **2012**, *64*, 475.
[35] I. H. Chen, W. Yang, M. A. Meyers, **2012**, unpublished.
[36] W. Yang, B. Gludovatz, E. A. Zimmermann, R. O. Ritchie, M. A. Meyers, unpublished.
[37] T. Y. Wu, *Annu.Rev. Fluid Mech.* **2011**, *43*, 25.
[38] D. W. Bechert, G. Hoppe, W.-E. Reif, *AIAA Paper* **1985**, *85–0546*, 1.
[39] D. Stuart-Fox, A. Moussalli, *Philos. Trans. Roy. Soc. Lond. B Biol. Sci.* **2009**, *364*, 463.
[40] W.-E. Reif, *ActaZool.-Stockholm* **1985**, *66*, 111.
[41] J. O. Farlow, C. V. Thompson, D. E. Rosner, *Science* **1976**, *192*, 1123.
[42] F. F. Torres, O. P. Troncoso, J. Nakamatsu, C. J.Grande, C. M. Gomez, *Mater. Sci. Eng.C* **2008**, *28*, 1276.
[43] Y.-S. Lin, C. T. Wei, E. A. Olevsky, M. A. Meyers, *J. Mech. Behav. Biomed. Mater.* **2011**, *4*, 1145.
[44] M. A. Meyers, Y. S. Lin, E. A. Olevsky, P.-Y. Chen, *Adv. Eng. Mater.* **2012**, *14*, B279.
[45] Y. Bouligand, *Tissue Cell* **1972**, *4*, 189.
[46] T. Ikoma, H. Kobayashi, J. Tanaka, D. Walsh, S. Mann, *J. Struct. Biol.* **2003**, *142 (3)*, 327.
[47] T. Ikoma, H. Kobayashi, J. Tanaka, D. Walsh, S. Mann, *Int. J. Biol. Macro.* **2003**, *32(3–5)*, 199.
[48] L. Zylberberg, G. Nicolas, *Cell Tissue Res.* **1982**, *223*, 349.
[49] L. Zylberberg, J. Bereiter-Hahn, J. Y. Sire, *Cell Tissue Res.* **1988**, *253*, 597.
[50] L. Zylberberg, J. Bonaventure, L. Cohen-Solal, D. J. Hartmann, J. Bereiter-Hahn, *J. CellSci.* **1992**, *103*, 273.
[51] L. Han, L. F. Wang, J. Song, M. C. Boyce, C. Ortiz, *Nano Lett.* **2011**, *11*, 3868.
[52] A. MarinaCugno Garrano, G. La Rosa, D. Zhang, L.-N. Niu, F. R. Tay, H. Majd, D. Arola, *J. Mech.Behav. Biomed. Mater.* **2012**, *7*, 17.
[53] T. M. Scheyer, P. M. Sander, *J. Vertebr. Paleontol.* **2004**, *24*. 874.
[54] J. O. Farlow, S. Hayashi, G. J. Tattersall, *Swiss J. Geosci.* **2010**, *103*, 173.
[55] S. Krauss, E. Monsonego-Ornan, E. Zelzer, P. Fratzl, R. Shahar, *Adv. Mat.* **2009**, *21*, 407.
[56] Y. Li, C. Ortiz, M. C. Boyce, *Phys. Rev. E* **2011**, *84*, 062904.
[57] The crack resistance-curve or R-curve provides an assessment of the fracture toughness in the presence of subcritical crack growth. It involves measurements of the crack-driving force, e.g., the stress intensity K or J-integral, as a function of crack extension (Δa). The value of the driving force at $\Delta a \rightarrow 0$ provides a measure of the crack-initiation toughness whereas the slope (used in this study) and/or the maximum value of the R-curve can be used to characterize the crack-growth toughness.
[58] Fracture resistance can be considered as a mutual competition between two classes of mechanisms: intrinsic mechanisms, which are microstructural damage mechanisms that operate ahead of the crack tip to promote cracking, and extrinsic mechanisms, which operate principally in the wake of the crack tip to inhibit cracking by "shielding" the crack from the applied driving force, see ref. [66]. Whereas intrinsic toughening mechanisms, e.g., plastic deformation, act in general to resist intrinsic microstructural damage and thus are effective in inhibiting both the initiation and growth of cracks, extrinsic toughening mechanisms, e.g., crack deflection and bridging, are only effective in inhibiting crack growth.
[59] K. J. Koester, J. W. Ager, R. O. Ritchie, *Biomaterials* **2008**, *29*, 1318.
[60] W. Yang, B. Gludovatz, E. A. Zimmermann, R. O. Ritchie, M. A. Meyers, unpublished.
[61] J. J. Pritchard, J. H. Scott, F. G. Girgis, *J. Anat.* **1956**, *90*, 73.
[62] F. J. Vernerey, F. Barthelat, *Int. J. Solids Struct.* **2010**, *47*, 2268.
[63] http://hotnewshome.com/2011/12/06/animal-pictures-of-the-year-2010-feeding-and-fighting/4950/attachment/ 4998
[64] http://www.pinnaclearmor.com/body-armor/dragon-skin/ (accessed October 2012); Image reproduced from Flexible Modular Body Armor Piercing Protection, Contract DAAD17-01-C-0028 from ARL Publication ARL-CR-257 by [Murray Neal & North American Development Group LLC].
[65] P. Fratzl, R. Weinkamer, *Prog. Mat. Sci.* **2007**, *52*, 1263–1334.
[66] R. O. Ritchie, *Nat. Mater.* **2011**, *10*, 817.